

# ANUBIS: Review and Benchmark Skeleton-Based Action Recognition Methods with a New Dataset

Zhenyue Qin, Yang Liu, Madhawa Perera, Saeed Anwar, Tom Gedeon, Pan Ji, Dongwoo Kim,

**Abstract**—Skeleton-based action recognition, as a subarea of action recognition, is swiftly accumulating attention and popularity. The task is to recognize actions performed by human articulation points. Compared with other data modalities, 3D human skeleton representations have extensive unique desirable characteristics, including succinctness, robustness, racial-impartiality, and many more. We aim to provide a roadmap for new and existing researchers on the landscapes of skeleton-based action recognition for new and existing researchers. To this end, we present a review in the form of a taxonomy on existing works of skeleton-based action recognition. We partition them into four major categories: (1) datasets; (2) extracting spatial features; (3) capturing temporal patterns; (4) improving signal quality. For each method, we provide concise yet informatively-sufficient descriptions. To promote more fair and comprehensive evaluation on existing approaches of skeleton-based action recognition, we collect ANUBIS, a large-scale human skeleton dataset. Compared with previously collected dataset, ANUBIS are advantageous in the following four aspects: (1) employing more recently released sensors; (2) containing novel back view; (3) encouraging high enthusiasm of subjects; (4) including actions of the COVID pandemic era. Using ANUBIS, we comparably benchmark performance of current skeleton-based action recognizers. At the end of this paper, we outlook future development of skeleton-based action recognition by listing several new technical problems. We believe they are valuable to solve in order to commercialize skeleton-based action recognition in the near future. The dataset of ANUBIS is available at: <http://hcc-workshop.anu.edu.au/webs/anu101/home>.

**Index Terms**—Action Recognition, Skeleton, Dataset, Survey.

## 1 INTRODUCTION

Action recognition is a long-standing important problem in human-centered computing and computer vision. This research field is attracting increasing attention since it is applicable to address extensive real-world vital problems, such as human-robot interaction, patient monitoring, sports analysis, and many more. We here describe three examples in detail.

- **Elderly care:** Populating aging is a global phenomenon. Globally, there are more than 700 million people aged 65 or over in 2019 [1]. This share is projected to rise further to 16% of the world population by 2050, where one in six people will be aged over 65 [1]. Caring for this increasing number of older people is becoming an increasingly serious problem. Ideally, we will build robots that accurately recognize older people’s behaviors to thoughtfully care for them.
- **Virtual reality:** Due to the COVID-19 restrictions starting from 2020, the market of virtual reality is experiencing a substantial raise. The global virtual reality market size is projected to achieve 84.09 billion USD before 2028 [2]. Action recognition techniques

play essential roles in implementing mature virtual reality systems. Computers are required to correctly understand the users’ body movements in order to give proper responses and interactions.

- **Security surveillance:** Security surveillance is a practical method to ensure the safety of people, buildings, and valuables [3]. It’s market size is projected to be 69.1 billion USD by 2026 [3]. Accurate action recognition is a key component of building smart surveillance systems to alleviate humans’ laborious efforts. These systems can help identify and prevent undesired activities such as fighting in school, crimes in airports and so on.

Recently, skeleton-based action recognition is rapidly accumulating popularity, supported by the high amount of recently published literature on this field. The problem is to recognize the action performed by a sequence of skeletons, where a skeleton is a collection of human articulations, with each articulation being associated with the 2D or 3D coordinates. The problem setting is visually depicted in Figure 1.

Currently, commercial sensors for estimating human skeletons can be obtained readily and cheaply. These devices accurately estimate human skeletons. Existing products include Microsoft Kinect sensors, Intel realsense depth cameras, and so on.

Compared with other modalities, 3D human skeleton sequences have a wide range of unique advantages. To illustrate, we list several here:

• Zhenyue Qin and Tom Gedeon were with Australian National University (ANU). Yang Liu, Madhawa Perera, and Saeed Anwar were with both ANU and Data61, CSIRO. Pan Ji was with OPPO US Research Center. Dongwoo Kim was with POSTECH.  
E-mail: zhenyue.qin@anu.edu.au.

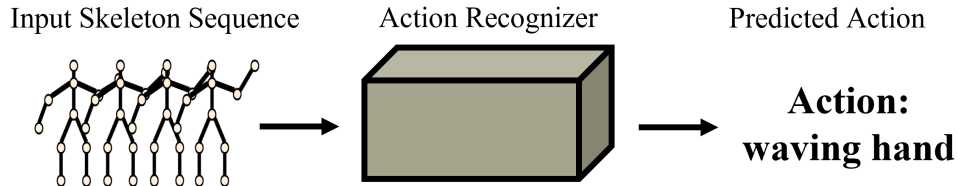


Fig. 1: Visual demonstration of skeleton-based action recognition.

- **Informative:** Biological work indicates that skeleton motion trajectories provide sufficient information for humans to recognize actions [4].
- **Succinct:** An action is succinctly represented by a sequence of the 3D joint sets, thus requiring small storage and supporting fast processing. For example, an action recognizer that utilizes the RGB videos has more than 118 million parameters. In comparison, the model using the skeleton data only has 0.69 million parameters. Furthermore, it takes more than 1 GB to record the RGB video for one minute. In contrast, recording the skeleton sequence for the same time merely consumes 500 KB.
- **Free of environmental influence:** Skeleton action sequences are clear of background, hence the action recognizer will be unaffected by background clutter, clothing, and lighting.
- **Privacy-protective:** Skeletons represent a human face as a single joint with 3D coordinates, hence effectively hiding critical identity information.
- **Racial-unbiased:** Skeletonized human bodies discard obvious racial features. This prevents a learning model from drawing unexpected correlations between races and actions.

We ultimately desire to achieve the commercialization of skeleton-based action recognition. We summarize our contributions as follows:

- We comprehensively review existing methods for skeleton-based action recognition and create their taxonomy as a roadmap for newly started or existing researchers.
- We collect a large-scale human skeleton dataset named ANUBIS. Using this dataset, we benchmark a variety of existing approaches for skeleton-based action recognition.
- We provide numerous potentially new directions

## 2 REVIEW OF EXISTING METHODS

In this section, we review the existing papers on skeleton-based action recognition. Among these papers, it is common that one paper makes multiple relatively independent contributions. For example, a single paper may simultaneously propose a newly-collected dataset as well as a novel temporal operator. For the sake of a more systematic overview from the perspective of the entire field, we organize this review section by contributions rather than papers. Following this principle, we classify different contributions from various papers into the following four major categories. Within each category, we further decompose it into subdivided

areas. We depict this hierarchically organized taxonomy as well as their descriptions as follows.

- **Datasets:** Collecting and releasing new human skeleton datasets.
- **Extracting spatial features:** Extracting the interacting relationships between joints within a skeleton.
  - **Leveraging topological structures:** Proposing new approaches of utilizing a skeleton’s topological information.
  - **Devising spatial operators:** Designing new operators that aggregate different joints’ information of a skeleton.
  - **Disentangling channel features:** Encouraging different channels of a model to learn semantically disentangled information.
  - **Learning parameterized topologies:** Creating learnable topological structures to improve the flexibility of aggregating spatial information.
  - **Partitioning hierarchical structures:** Endowing prior knowledge about the human structure to the model by partitioning a skeleton into different spatial groups.
  - **Applying novel architectures:** Devising new architectures for aggregating spatial information.
- **Capturing temporal patterns:** Capturing dynamical information between frames along time.
  - **Extracting multiscale features:** Extracting temporal dynamics of multiple scales.
  - **Designing temporal operators:** Devising new approaches of fusing temporally dynamical information.
  - **Selecting informative frames:** Emphasizing the frames that are more informative than the other frames.
- **Improving signal quality:** Enhancing the data quality of skeleton sequences.
  - **Encoding semantic information:** Fusing prior knowledge about joints’ semantic information.
  - **Transforming geometric coordinates:** Transforming joint coordinates to a standard coordinate system.
  - **Mitigating overfitting problems:** Improving the model’s generalizability.
  - **Designing new features:** Proposing novel features as additional inputs.

As an overview, the following list shows the affiliation relationships between different methods and the above hierarchy.

- **Datasets:** [5], [6], [7], [8], [9], [10], [11], [12], [13], [14], [15], [16] [17]
- **Extracting spatial features:**
  - **Leveraging topological structures:** [18], [19], [20], [21], [22], [23], [24], [25].
  - **Devising spatial operators:** [26], [27], [28], [29], [30]
  - **Disentangling channel features:** [31], [32]
  - **Learning parameterized topologies:** [33], [34], [35], [36], [37],
  - **Partitioning hierarchical structures:** [38], [11], [39], [40], [36]
  - **Applying Novel Architectures:** [41], [42], [43], [44], [45], [46], [47], [48]
- **Capturing temporal patterns:**
  - **Extracting multiscale features:** [49]
  - **Designing temporal operators:** [40], [50], [25],
  - **Selecting informative frames:** [51], [52]
- **Improving signal quality:**
  - **Encoding semantic information:** [53]
  - **Transforming geometric coordinates:** [54], [49], [14], [55]
  - **Mitigating overfitting problems:** [31]
  - **Designing new features:** [56], [57]

In the rest of this section, we dive into details of a proportion of existing approaches listed above.

### 3 DATASETS

#### 3.1 MSR Action3D

The MSR Action3D dataset [6] was collected by Microsoft Kinect depth cameras. It contains 20 actions, performed by 10 subjects two or three times. The dataset totally consists of 557 action sequences. The skeleton in each sequence’s frame comprises 20 joints. The challenges for accurately recognizing these skeletons’ actions lie in the poorly estimated coordinates and missed partial fragments.

#### 3.2 Berkeley MHAD

The Berkeley MHAD dataset [10] was captured by a motion capture system. It totally comprises 659 action sequences with approximately 82 minutes of recording. The actions were performed by 7 males and 5 females, with each action being repeated five times. The skeleton of each frame contains 35 joints.

#### 3.3 Motion Capture Dataset HDM05

The HDM05 dataset [5] was collected by an optical marker-based technology with the frequency of 120 Hz. It consists of 65 action categories and 2337 sequences acted by five participants.

#### 3.4 SBU Interaction

The SBU Interaction dataset [7] consists of eight two-person interacting actions collected with Microsoft Kinect sensors. It comprises 282 sequences and 6822 frames. Each skeleton contains 15 joints. All videos were recorded under the same laboratory environment performed by 7 participants.

#### 3.5 UTKinect Action3D

The UTKinect Action3D dataset [8] was collected using a single Microsoft Kinect camera. It consists of 10 action types performed by 10 subjects. Each subject performed each action twice. Each estimated skeleton has 20 joints.

#### 3.6 CMU

The CMU dataset [9] contains 2235 sequences and approximately 1 million frames. It has 45 action classes performed by a single person. Each skeleton includes 31 joints.

#### 3.7 Northwestern-UCLA

The Northwestern-UCLA dataset [12] was captured by three Microsoft Kinect cameras simultaneously from various viewpoints. The actions were performed by 10 subjects, including 1494 video clips covering 10 categories. Samples from two cameras are for training and the others are for validation.

#### 3.8 UWA3DII

The UWA3DII dataset [14] was collected by four Microsoft Kinect sensors. It consists of 30 actions performed by ten subjects. Each action is repeatedly performed four times, recorded from four views: left and right side views as well as front and top views.

#### 3.9 SYSU 3D Human-Object Interaction

The SYSU 3D Human-Object Interaction dataset (SYSU) [13] contains 480 skeleton sequences and 12 actions performed by 40 different subjects. There are two evaluation protocols for this dataset: the cross subject (CS) and the same subject (SS). For CS, half of the subjects are used for training and the remaining for testing. For SS, half of the skeleton sequences of each activity are used for training and the rest for testing.

#### 3.10 Kinetics

The Kinetics dataset [15] is collected from more than 250,000 YouTube videos. The raw videos of the Kinetics dataset are collected from YouTube. Then, the skeletons are estimated with the OpenPose algorithm [58]. Each comprises 18 joints and their 3D coordinates. These skeletons are split into a training set of size 240,436 and a validation set of size 19,796. Unlike NTUs, skeleton sequences from this dataset suffer from occlusion problems, including partial occlusion of human subjects by other subjects and self-occlusion of human subjects themselves. Furthermore, each skeleton uses only one joint to represent the hand region, which makes it hard for fine-grained action recognition, especially when the actions mainly relying on two hands (*e.g.* cooking, cutting and slicing).

#### 3.11 NTU60

NTU60 [11] is a widely-used benchmark dataset for skeleton-based action recognition, incorporating more than 56,000 videos and 4 million frames. The action videos were collected in a laboratory environment with Microsoft Kinect V2 cameras, resulting in accurately extracted skeletons,

each comprising 25 joints. It totally contains more than 56 thousand sequences and 4 million frames. The action list covers various scenarios, including daily individual and interactive behaviors as well as medical conditions. These actions were performed by 40 subjects aged between 10 and 35. The actions were recorded by three cameras located with three views facing to the subject: right to the person and diagonally facing to the person with  $\pm 45^\circ$ .

On the other hand, recognizing actions from these relatively high-quality skeletons is challenging due to five aspects: the skeletons are captured from different viewpoints; the skeleton sizes of subjects vary; so do their speeds of action; different actions can have similar motion trajectories; there are limited joints to portray hand actions in detail.

The authors [11] recommend evaluating the recognizing accuracy under two settings: (1) cross-subject (XSub), where the entire 40 subjects are evenly split into training and validating groups, yielding 40,320 sequences for training and 16,560 for validation. (2) cross-view (XView), where the sequences captured from the cameras that directly face and  $+45^\circ$  orient toward the subject are for training (37,920 instances), and the rest from the  $-45^\circ$  orientation view are for validation (18,960 instances).

### 3.12 NTU120

NTU120 [16] is an extension of NTU60 with an additional 57,367 skeleton sequences and 60 extra action categories. This amounts to the totaling 113,945 samples and 120 classes. These actions were performed by 106 distinct subjects and 32 different camera setups. As for the evaluation protocols, the authors recommend substituting the cross-setup (XSet) for the original cross-view (XView). The new setting uses more camera positions and angles. Specifically, 54,468 skeleton sequences obtained from half of the camera setups are utilized for training and the other 59,477 samples are for validation. For the cross-subject setting, 63,026 skeleton sequences collected from 53 subjects are used for training, and the rest 50,919 samples are for validation.

## 4 EXTRACTING SPATIAL FEATURES

### 4.1 Leveraging Topological Structures

**Disentangling Neighborhoods:** In [25], as conceptually depicted in the (c) part of Figure 2, the authors propose a new multi-scale aggregation approach. Instead of repeatedly aggregating more distant joints' features, the authors create diverse adjacency matrices. Each matrix extracts interacting patterns of joints with a certain distance. This scheme removes duplicated dependencies between further and closer neighborhoods.

Mathematically, the authors define the  $k$ -adjacency matrix  $\tilde{\mathbf{A}}_{(k)}$  as

$$[\tilde{\mathbf{A}}_{(k)}]_{i,j} = \begin{cases} 1 & \text{if } d(v_i, v_j) = k, \\ 1 & \text{if } i = j, \\ 0 & \text{otherwise,} \end{cases} \quad (1)$$

where  $d(v_i, v_j)$  is the shortest distance in number of hops between  $v_i$  and  $v_j$ .  $\tilde{\mathbf{A}}_{(k)}$  is a generalized form of  $\tilde{\mathbf{A}}$  to further neighborhoods, with  $\tilde{\mathbf{A}}_{(1)} = \tilde{\mathbf{A}}$  and  $\tilde{\mathbf{A}}_{(0)} = \mathbf{I}$ . Given that the number of nodes is small,  $\tilde{\mathbf{A}}_{(k)}$  can be easily computed,

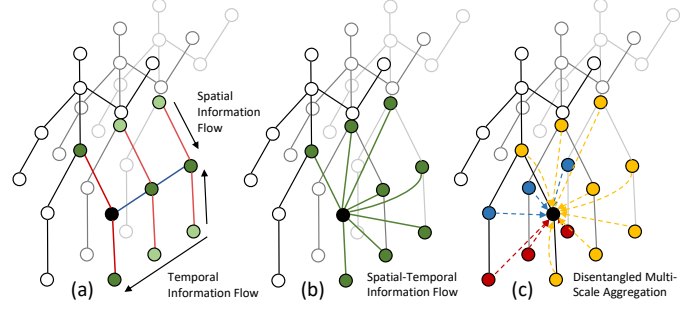


Fig. 2: (a) *Indirect* spatial-temporal information flow. (b) G3D to capture cross-spacetime correlations with *unified* spatial-temporal graph convolutions. (c) Disentangling node features at separate spatial-temporal neighborhoods (yellow, blue, red) with distant distances, for multi-scale learning in the spatial domain. The image is from [25].

e.g., utilizing differences of graph powers as:  $\tilde{\mathbf{A}}_{(k)} = \mathbf{I} + \mathbb{1}(\tilde{\mathbf{A}}^k \geq 1) - \mathbb{1}(\tilde{\mathbf{A}}^{k-1} \geq 1)$ . Substituting  $\tilde{\mathbf{A}}^k$  with  $\tilde{\mathbf{A}}_{(k)}$  in the GCN operation form proposed in [59], we arrive at:

$$\mathbf{X}_t^{(l+1)} = \sigma \left( \sum_{k=0}^K \tilde{\mathbf{D}}_{(k)}^{-\frac{1}{2}} \tilde{\mathbf{A}}_{(k)} \tilde{\mathbf{D}}_{(k)}^{-\frac{1}{2}} \mathbf{X}_t^{(l)} \Theta_{(k)}^{(l)} \right), \quad (2)$$

where  $\tilde{\mathbf{D}}_{(k)}^{-\frac{1}{2}} \tilde{\mathbf{A}}_{(k)} \tilde{\mathbf{D}}_{(k)}^{-\frac{1}{2}}$  is the normalized  $k$ -adjacency.

**DGNN:** [24] proposes a directed graph neural network to more adequately capture the dependencies between joints and their connected bones. The directed graph model straightforwardly characterizes the topological dependencies to comprehensively extract complex interacting patterns between joints. The internal hierarchies of a directed graph also explicitly enable learning features with diverse levels of abstractions.

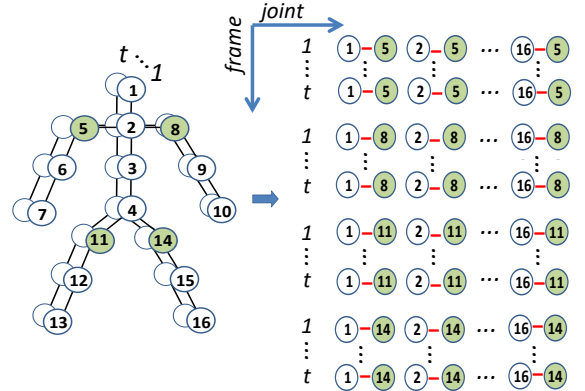


Fig. 3: Visual demonstration of converting a skeleton to the cylindrical coordinate representations. The image is from [20].

**C-CNN:** In [20], the authors propose to leverage CNNs to broadly extract spatial and temporal patterns of a skeleton sequence. Since the relative positions between joints provide more kinetic information than the absolute positional coordinates, the authors use the cylindrical coordinates between



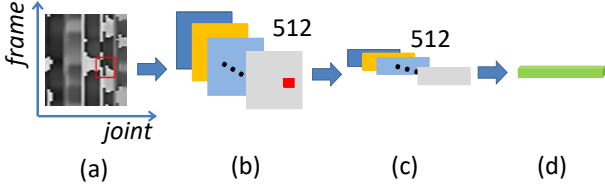


Fig. 4: Illustration of CNN feature extraction and temporal mean pooling. The image is from [20].

each joint and four reference joints. The reference ones are intended to be stable for most actions. The authors choose them as the left shoulder, the right shoulder, the left hip and the right hip. The transformation procedure is visually depicted in Figure 3. A skeleton from a frame is converted to four 2D images. Each corresponds to a reference point.

This conversion equally applies to each dimension of the 3D coordinates. For each reference point, the 2D images from different dimensions are jointly concatenated. That is, each joint accordingly corresponds to a multi-channel 2D image. The subsequent procedure is pictorially demonstrated in Figure 4. The produced image is fed to a pretrained VGG19 [60] model. In the end, temporal pooling is equally performed for every channel. The resultant pooled features are eventually concatenated.

The entire architecture is shown in Figure 5. The total loss value is the summation of the loss for each of the four components.

**ST-LSTM:** The spatio-temporal long short-term memory (ST-LSTM) network proposed in [19] extends the recurrent analysis toward the spatial domain, in parallel to the original temporal direction. The new iteration over the spatial domain is to explore the spatial co-occurrences between joints in each frame. The procedure is pictorially demonstrated in Figure 6. Along the spatial direction, each ST-LSTM unit corresponds to a skeleton joint. During the feed-forwarding process, unit of joint  $j$  at time  $t$  is fed jointly with its own features  $\mathbf{x}_{j,t}$ , as well as the hidden representations of previous joint  $j-1$  ( $\mathbf{h}_{j-1,t}$ ) and past time frame  $t-1$  ( $\mathbf{h}_{j,t-1}$ ) to adequately capture the local movement pattern. Additionally, joint  $j$  also receives information of both spatial and temporal forget gates ( $f_{j,t}^S$  and  $f_{j,t}^T$ ) as more global contextual information. The exact procedure for updating cell  $c_{j,t}$  and hidden state  $h_{j,t}$  of a LSTM unit is mathematically formulated as:

$$\begin{pmatrix} i_{j,t} \\ f_{j,t}^S \\ f_{j,t}^T \\ o_{j,t} \\ u_{j,t} \end{pmatrix} = \begin{pmatrix} \sigma \\ \sigma \\ \sigma \\ \sigma \\ \tanh \end{pmatrix} \left( M \begin{pmatrix} x_{j,t} \\ h_{j-1,t} \\ h_{j,t-1} \end{pmatrix} \right)$$

$$c_{j,t} = i_{j,t} \odot u_{j,t} + f_{j,t}^S \odot c_{j-1,t} + f_{j,t}^T \odot c_{j,t-1}$$

$$h_{j,t} = o_{j,t} \odot \tanh(c_{j,t}).$$

The authors further encodes the skeleton’s adjacency relationship in the visiting order of joints along the spatial recurrence. To this end, the traversal path is generated by the bidirectional depth-first search manner with the spine joint as the root.

The entire architecture is visually illustrated in Figure 8.

## 4.2 Devising Spatial Operators

**ST-GCN:** The spatial-temporal graph convolutional network is the pioneering work that effectively leverages the graph network to elegantly incorporate human structural information. The processing pipeline separately handles the spatial and temporal features. The graph convolution is applied to spatially aggregate topological information. Along with the temporal direction, 1x1 convolutions are utilized to capture motion patterns. Figure 9 visually demonstrate the architecture’s pipeline.

**Shift-GCN:** The shift graph convolutional network (shift-GCN) [30] presents a new scheme for aggregating joint features of a graph neural network. They introduce the shift operator to graph neural networks. The proposed shift operation consists of two types. First, the local one. For a joint, when extracting its neighbors’ features, the joint swaps its partial embedding with that of its neighbors. Second, the global one. Exchanging embeddings happen to all pairs of joints within a skeleton. Replacing the traditional graph convolution with the new graph shift operation, the GFLOPs can be hugely reduced. Figure 10 and Figure 11 visually describe the operating details of the shift-GCN.

**AGC-LSTM:** [28] proposes the attention enhanced graph convolutional LSTM network (AGC-LSTM) that mixes recurrent neural networks and graph neural networks, in order to effectively capture the complex spatial-temporal movement patterns of human skeletons.

The overview architecture of the proposed model is a long short-term memory network, as displayed in Figure 12. The operations of their various internal gates are graph aggregators, described in more detail in Figure 13 and Figure 14. The attention mechanism is applied to more efficiently extract information from more prominent joints, visually depicted in Figure 15. A joint integrates more features from its neighbors with more affinity.

To more comprehensively learn multiscale interacting patterns of a skeleton, the part-based skeleton graph is also employed. The skeleton graph is partitioned into several functional groups such as arms and legs. The joint- and part-based skeletons go through two separate models, then the two outputs are fused to produce the final prediction.

## 4.3 Disentangling Channel Features

**Decoupling GCN:** [31] aims to extract diverse interaction patterns between joints. Previous approaches rigidly utilize one single topology to extract and aggregate every dimension’s features. However, different dimensions may represent distinct motion patterns. Thus, [31] proposes the decoupling GCN to apply divergent topological structures to integrate features in different channels, aiming to more flexibly model complex motion patterns.

**CTR-GCN:** The channel-wise topology refinement graph convolution network (CTR-GCN) [32] intends to let the graph convolutional network learn topologies of different channels. Most previous algorithms that leverage GCNs for

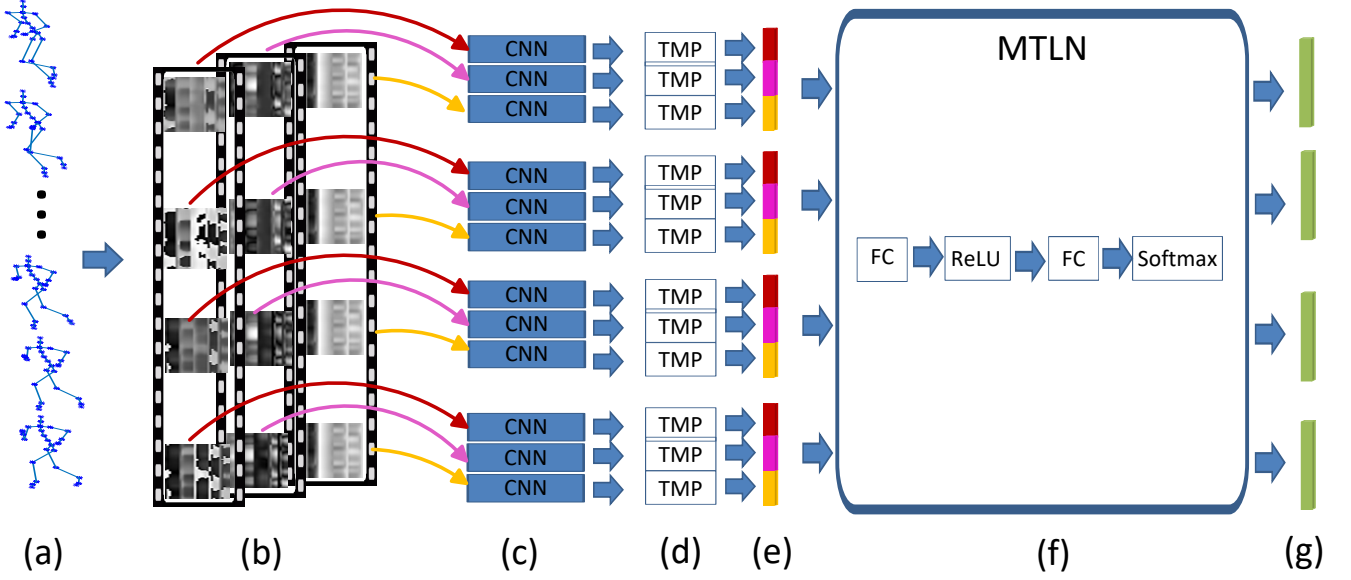


Fig. 5: Exhibition of the architecture in [20]. The image is from [20].

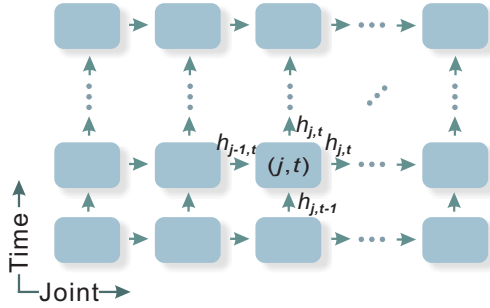


Fig. 6: The visual demonstration of the proposed spatio-temporal LSTM network [19]. Along the spatial direction, joints' features are sequentially fed in a predefined order. In the temporal evolving direction, joints' features are consecutively processed. Each unit also takes the previous spatial and temporal information as the contextual clues. The figure is from [19].

skeleton-based action recognition apply a single topology for all channels. This causes GCNs to use the same topology to aggregate features of different channels. Using a single topology limits the flexibility of feature extraction, since different kinds of motion features and joint correlations are represented in distinct channels. It requires divergent topological structures to fuse different kinds of information. DecoupleGCN is the pioneering work learning a unique topology for each individual channel. These topologies are learned independently from the node features. In contrast, CTR-GCN dynamically generates topologies using the joint features. The generating function considers both the difference and concatenation of features. Given  $\psi$  and  $\phi$  are two linear functions for dimension reduction, the exact form is:

$$M_1(\psi(\mathbf{x}_i), \phi(\mathbf{x}_j)) = \sigma(\psi(\mathbf{x}_i) - \phi(\mathbf{x}_j)), \quad (3)$$

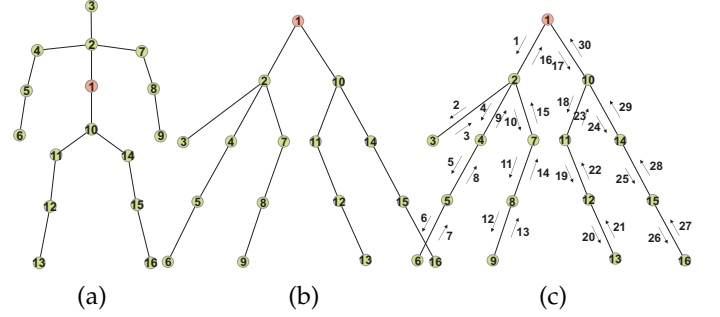


Fig. 7: (a) Skeleton joints. (b) Tree representation of a skeleton. (c) Tree traversal of the spatial visiting order: 1-2-3-2-4-5-6-5-4-2-7-8-9-8-7-2-1-10-11-12-13-12-11-10-14-15-16-15-14-10-1. The figure is from [19].

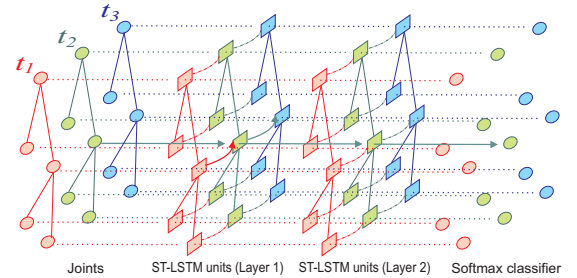


Fig. 8: ST-LSTM's architecture [19]. The image is from [19].

and

$$M_2(\psi(\mathbf{x}_i), \phi(\mathbf{x}_j)) = f(\psi(\mathbf{x}_i) \parallel \phi(\mathbf{x}_j)), \quad (4)$$

where  $\parallel$  is concatenation operation and  $f$  is a multi-layer perceptron. Then, the channel-specific correlations  $\mathbf{Q} \in \mathbb{R}^{N \times N \times C'}$  are obtained by employing linear transformation

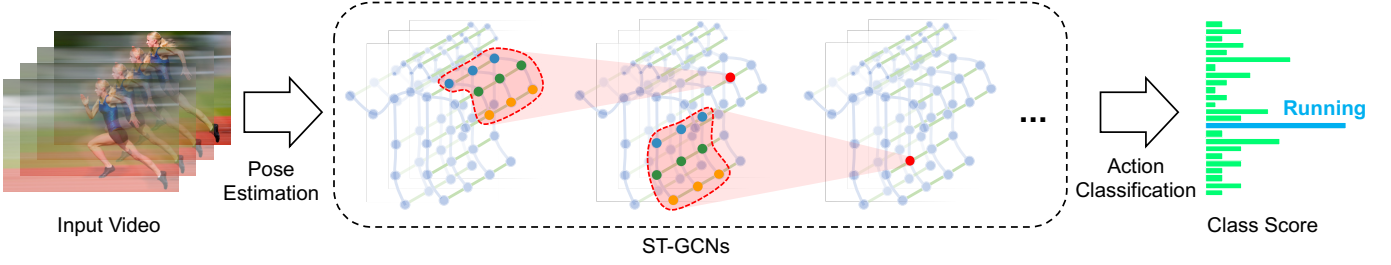


Fig. 9: Pipeline of the spatial-temporal graph neural network (ST-GCN) [61]. Multiple layers of spatial-temporal graph convolutions are utilized to gradually capture higher-level action features. The image is from [61].

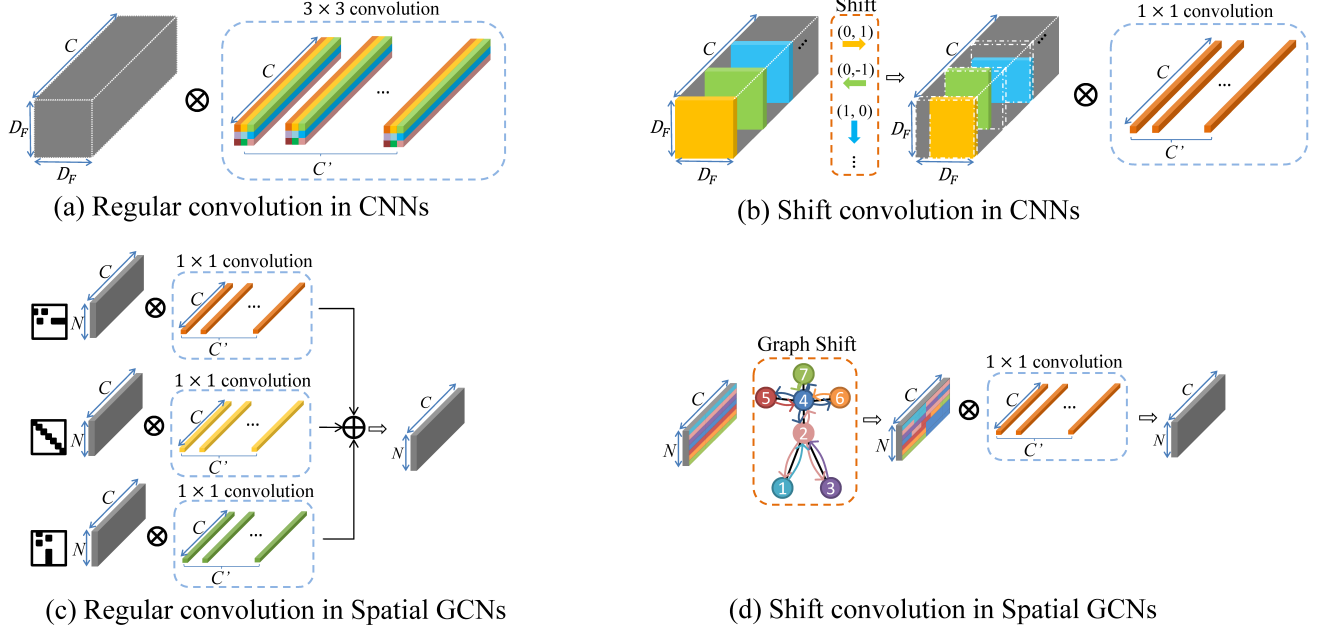


Fig. 10: Comparison between the CNN and GCN's operators. The image is from [30].

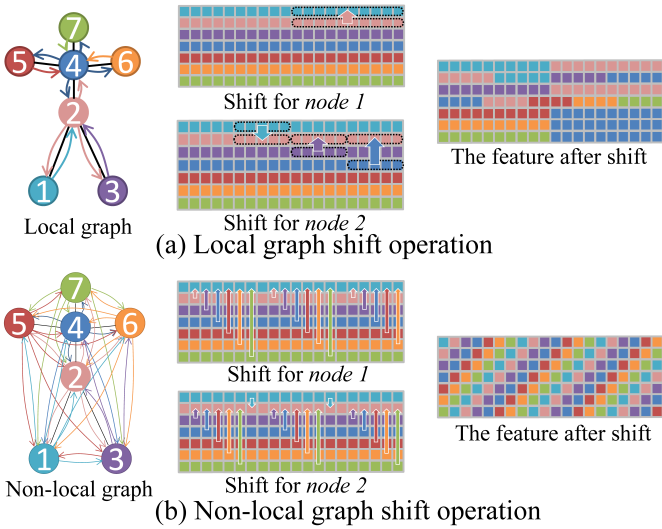


Fig. 11: Visual illustration of the shift-GCN's operations. The image is from [30].

$\xi$  to enlarge the channel dimension:

$$\mathbf{q}_{i,j} = \xi(M(\mathbf{x}_i), \phi(\mathbf{x}_j)), i, j \in \{1, 2, \dots, N\}, \quad (5)$$

where  $\mathbf{q}_{i,j}$  reflects a channel-specific topological relationship between  $v_i$  and  $v_j$ .

Apart from the dynamically generated channel-wise topologies, there is also a learnable topology matrix  $\mathbf{A}$  that is shared by all the channels. Eventually, the final topology  $\mathbf{R}$  is expressed as:

$$\mathbf{R} = \mathbf{A} + \alpha \cdot \mathbf{Q}, \quad (6)$$

where  $\alpha$  is a trainable scalar to control the intensity of refinement. Then, all the channel-wise topologies are concatenated together.

The concept is pictorially demonstrated in Figure 16. The architecture is visually depicted in Figure 17.

#### 4.4 Learning Parameterized Topologies

**CA-GCN:** Existing graph-based methods apply a manually predefined topology to extract interacting patterns of skeleton joints. This rigid topology ignores many interconnections between joints. To enrich learning more various

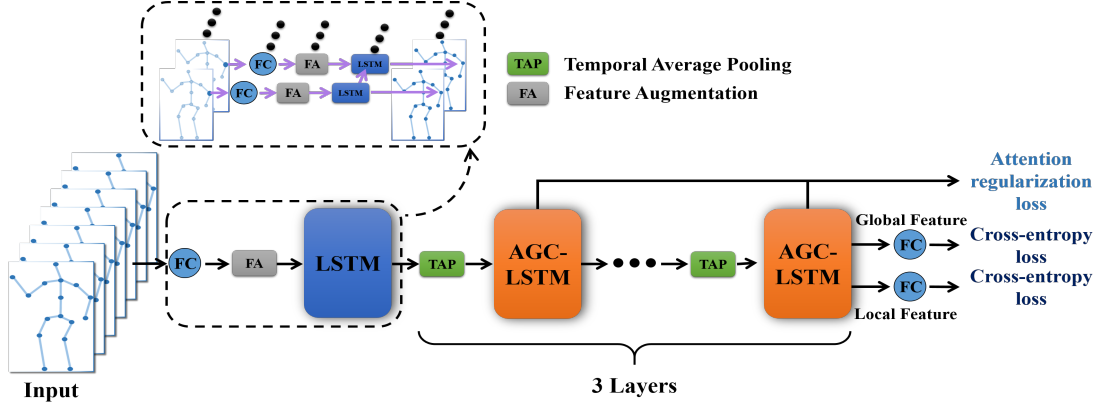


Fig. 12: Illustration of the AGC-LSTM's architecture. Both the global features of all joints and the local features of focused joints are jointly utilized to predict the action class. This image is from [28].

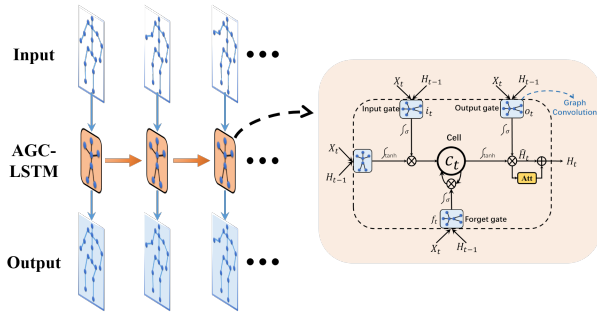


Fig. 13: Visualization of a single layer of the AGC-LSTM. This image is from [28].

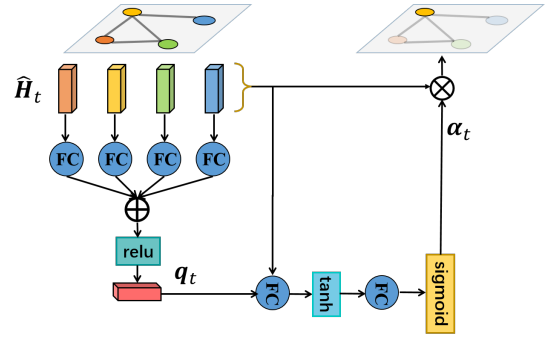


Fig. 15: Visual demonstration of the spatial attention network. This image is from [28].

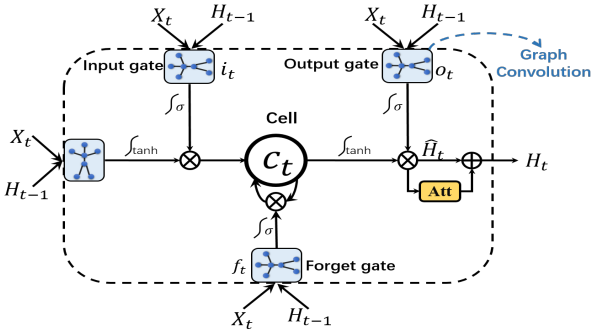


Fig. 14: Visualization of an AGC-LSTM's unit. This image is from [28].

interacting patterns between joints, [35] proposes context-aware graph convolutional networks (CA-GCNs). When integrating one joint's feature, instead of only aggregating from its manually predefined neighbors, the CA-GCN updates the joint's feature using all the joints' representations. Similar to the ideas of non-local or attention mechanisms, The contribution from one joint to another is determined by the relevance function. Depending on the form of this relevance function, a CA-GCN can be implemented as a light version and an advanced version.

- 1) Light version: The authors offer three forms of the relevance function:
  - a) Inner product between two node features.

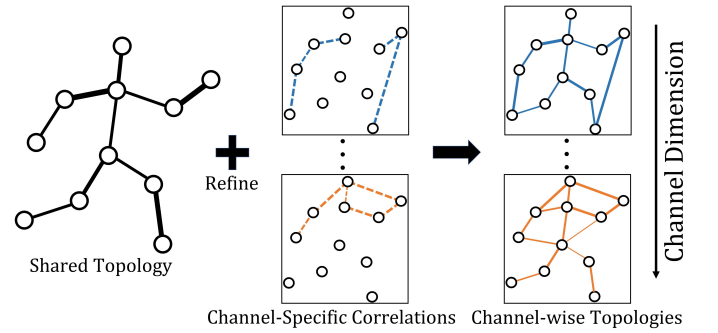


Fig. 16: Channel-wise topology refinement. Lines with distinct colors represent topologies of distinct channels. The line thickness indicates the correlation strength between joints. The image is from [32].

- b) Bilinear form of two node features.
  - c) Trainable relevance score of two node features. That is, using a learnable function to explicitly learn the relevance scores.
- 2) Advanced version: The authors claim that the original features of joints may not be suitable for directly evaluating the relevance. Thus, when estimating the relevance between two joints, one joint is defined to be the sender and the other is the receiver. Both the sender and the receiver's features undertake an



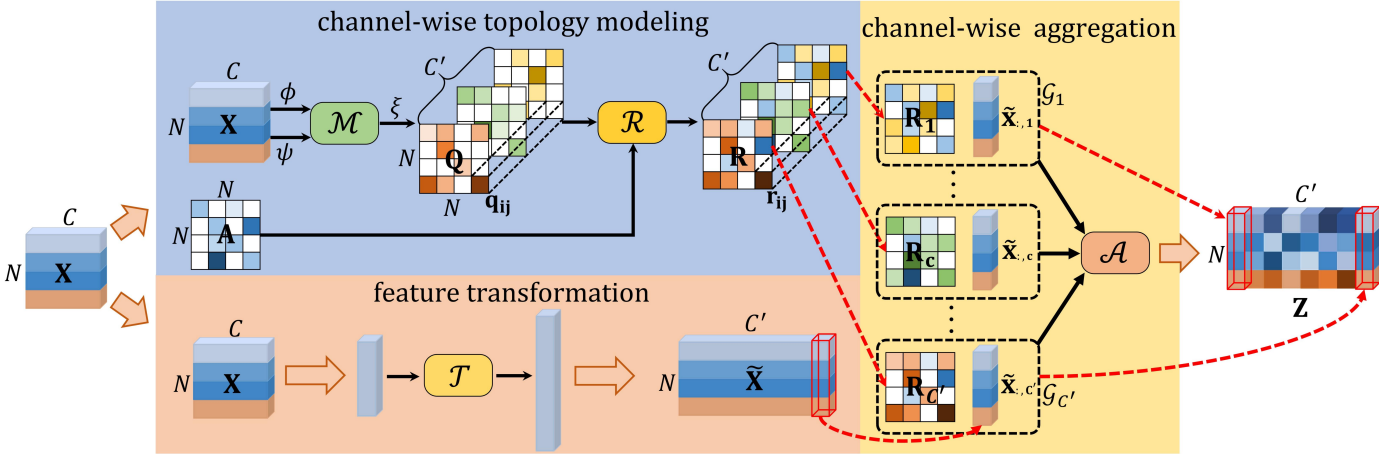


Fig. 17: Visualization of the CTR-GCN's architecture. The image is from [32].

affine transformation, followed by using a relevance function to evaluate the two joints' affinity.

**2S-AGCN:** The two-stream adaptive graph convolutional network proposed in [34] aims to flexibly learn the structural information of skeletons instead of rigidly sticking to using a manually defined structure for skeleton-based action recognition. The proposed new topology unifies three types of adjacency matrices in the form of summation. The three matrices are:

- 1) The physical structure of the human body.
- 2) A tunable adjacency matrix.
- 3) A data-dependent graph. The interaction between two joints is dynamically determined by the two's features, written as below:

$$f(v_i, v_j) = \frac{\exp \theta(v_i)^T \phi(v_j)}{\sum_{i=1}^N \exp \theta(v_i)^T \phi(v_j)}, \quad (7)$$

where  $v_i$  and  $v_j$  are two joints, and  $\theta$  and  $\phi$  are two functions.

[34] also explores second-order temporal features, additionally exploits the difference between two adjacent joints as new bone features. Feeding these bone features in a supplementary information flow along with the original joint feature path steadily improves the final prediction. The process is visually illustrated in Figure 18.

**AS-GCN:** The actional-structural graph convolutional network (AS-GCN) [33] collaboratively employ two types of topological structures:

- 1) Structural links (S-links), explicitly derived from the human body topology;
- 2) Actional links (A-links), directly inferred from skeleton data.

Figure 19 visually describe the overall pipeline of the proposed AS-GCN. Figure 20 illustrates S-links and A-links for the action walking.

**Actional-Links (A-Links):** Many actions are in conjunction performed by two far-apart joints. AS-GCN introduces actional links to directly capture these distant dependencies.

These actional links are adaptively generated using a trainable A-link inference module (AIM). An AIM consists of an encoder and a decoder.

**Encoder:** The encoder's functionality is to dynamically estimate  $C$  types of A-links based on the input joints' features. The procedure is to first extract link features from 3D positions, followed by converting these link features to probabilities. In the  $k$ -iteration, the encoder back and forth propagate information between joints and links. Figure 21 presents a visual description of the autoencoder for extracting A-links. Mathematically, the process can be written as follows:

$$\begin{aligned} \text{link features : } \mathbf{Q}_{i,j}^{(k+1)} &= f_e^{(k)}(f_v^{(k)}(\mathbf{p}_i^{(k)}) \oplus (f_v^{(k)}(\mathbf{p}_j^{(k)}))), \\ \text{joint features : } \mathbf{p}_i^{(k+1)} &= \mathcal{F}(\mathbf{Q}_{i,:}^{(k+1)}) \oplus \mathbf{p}_i^{(k)}, \end{aligned}$$

where  $i$  and  $j$  represent the indices of joints,  $f_v(\cdot)$  and  $f_e(\cdot)$  are both multi-layer perceptrons,  $\oplus$  indicates concatenation, and  $\mathcal{F}(\cdot)$  is an operation to integrate link features and obtain the joint feature; such as averaging and elementwise maximization. After  $K$  times of iterations, the output link probabilities are:

$$\mathcal{A}_{i,j,:} = \text{softmax} \left( \frac{\mathbf{Q}_{i,j}^{(K)} + \mathbf{r}}{\tau} \right) \in \mathbb{R}^C, \quad (8)$$

where  $\mathbf{r}$  are i.i.d. sampled from Gumbel(0,1) distribution [62] and  $\tau$  controls the discretization of  $\mathcal{A}_{i,j,:}$ .

Then, the authors propose the actional graph convolution (AGC) to aggregate and transform joint features using the ad hoc generated A-links. Given the input  $\mathbf{X}_{\text{in}}$ , the AGC's mathematical form is:

$$\begin{aligned} \mathbf{X}_{\text{act}} &= \text{AGC}(\mathbf{X}_{\text{in}}) \\ &= \sum_{c=1}^C \hat{\mathbf{A}}_{\text{act}}^{(c)} \mathbf{X}_{\text{in}} \mathbf{W}_{\text{act}}^{(c)} \in \mathbb{R}^{n \times d_{\text{out}}}, \end{aligned} \quad (9)$$

where  $\hat{\mathbf{A}}_{\text{act}}^{(c)} = \mathbf{D}_{\text{act}}^{(c)-1} \mathbf{A}_{\text{act}}^{(c)}$ ,  $\mathbf{D}$  is the diagonal degree matrix to normalize the graph convolution,  $\mathbf{W}_{\text{act}}^{(c)}$  is the trainable weight to capture feature importance.

**Decoder:** The decoder's functionality is to predict the future 3D motion trajectory given the previous action sequence. The intuition is to adequately preserve dynamic

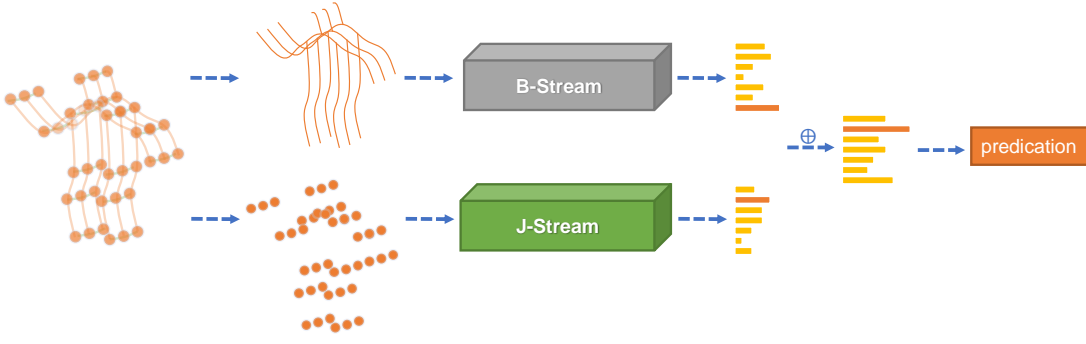


Fig. 18: Illustration of 2s-AGCN's overall architecture. J and B stand for joint and bone respectively. This image is from [34].

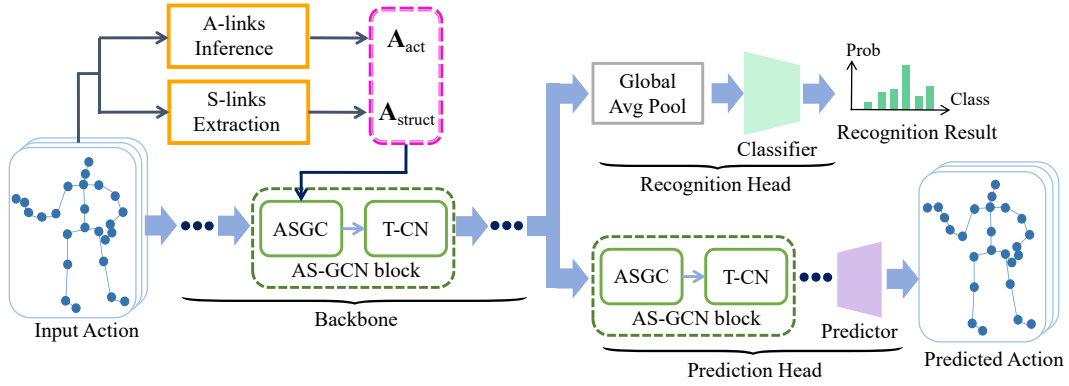


Fig. 19: The overall pipeline of the AS-GCN [33]. An actional-structural graph convolution (ASGC) simultaneously utilize two types of links (A-links and S-links) to comprehensively extract the spatial interacting patterns between joints. The final outputs are produced by two parallel branches: the recognition head for action recognition and the prediction one for forecasting future motion trajectories. The image is from [33].

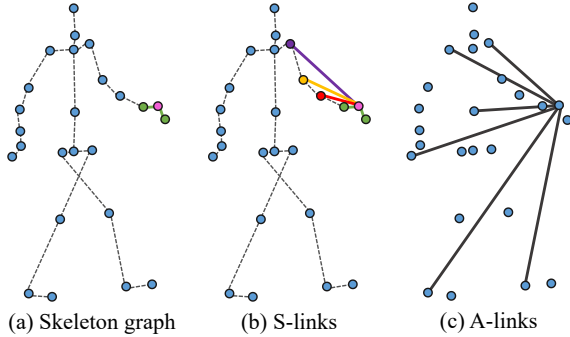


Fig. 20: An illustration of different skeleton links for the action walking. The image is from [33].

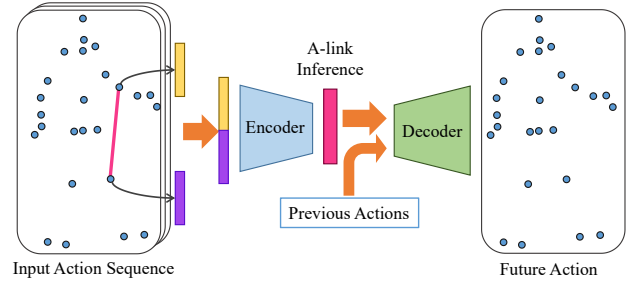


Fig. 21: A-links inference module (AIM) [33]. To extract the A-links, the concatenated joint features are fed into the encoder to produce the A-links. The decoder anticipates the future poses conditioned on both the A-links and previous actions. The image is from [33].

details of the motion sequence. The decoder's mathematical form consists of the following four components:

$$\begin{aligned}
 (a) \quad \mathbf{Q}_{i,j}^t &= \sum_{c=1}^C \mathcal{A}_{i,j,c} f_e^{(c)}(f_v^{(c)}(\mathbf{x}_i^t) \oplus f_v^{(c)}(\mathbf{x}_j^t)) \\
 (b) \quad \mathbf{p}_i^t &= \mathcal{F}(\mathbf{Q}_{i,:}^t) \oplus \mathbf{x}_i^t \\
 (c) \quad \mathbf{S}_i^{t+1} &= \text{GRU}(\mathbf{S}_i^t, \mathbf{p}_i^t) \\
 (d) \quad \hat{\mu}_i^{t+1} &= f_{\text{out}}(\mathbf{S}_i^{t+1}) \in \mathbb{R}^3,
 \end{aligned}$$

where  $f_v^{(c)}(\cdot)$ ,  $f_e^{(c)}(\cdot)$  and  $f_{\text{out}}(\cdot)$  are MLPs, GRU stands for a gated recurrent unit.

The authors also state that a sparse structure substantially boosts the performance.

**Structural Links (S-Links):** The authors define the structural graph convolution (SGC) to directly capture the long-range dependencies using the high-order polynomial of  $\mathbf{A}$ . The SGC is represented as:

$$\begin{aligned}
 \mathbf{X}_{\text{struc}} &= \text{SGC}(\mathbf{X}_{\text{in}}) \\
 &= \sum_{l=1}^L \sum_{p \in \mathcal{P}} \mathbf{M}_{\text{struc}}^{(p,l)} \circ \hat{\mathbf{A}}^{(p)l} \mathbf{X}_{\text{in}} \mathbf{W}_{\text{struc}}^{(p,l)} \\
 &\in \mathbb{R}^{n \times d_{\text{out}}},
 \end{aligned} \tag{10}$$

where  $l$  is the polynomial order. The trainable parameters  $\mathbf{M}_{\text{struc}}^{(p,l)} \in \mathbb{R}^{n \times n}$  and  $\mathbf{W}_{\text{struc}}^{(p,l)} \in \mathbb{R}^{n \times d_{\text{struc}}}$  are incorporated to flexibly weight more for more discriminative features.

*Fusing A-Links and S-Links:* The authors cohesively aggregate the AGC and SGC as the actional-structural graph convolution (ASGC) to comprehensively extract both actional and structural motion patterns. The ASGC operation is formulated as:

$$\begin{aligned}\mathbf{X}_{\text{out}} &= \text{ASGC}(\mathbf{X}_{\text{in}}) \\ &= \mathbf{X}_{\text{struc}} + \lambda \mathbf{X}_{\text{act}} \in \mathbb{R}^{n \times d_{\text{out}}},\end{aligned}$$

where  $\lambda$  is a hyper-parameter.

**MV-IGNet:** The multi-View interactional graph network (MV-IGNet) [36] is proposed to construct, learn and infer multi-level spatial skeleton context, including view-level (global), group-level, join-level (local) context, in a unified way.

MV-IGNet utilizes different skeleton topologies as multi-view to cooperatively produce complement cues of different actions. These different views extract multi-level interaction patterns of skeleton actions.

(1) Joint-level (local) view depicts the interactions between one joint and its neighbors. Existing GCN-based methods transform the node features in a weight-sharing approach. This implies all pairs of joints have the same interacting patterns. However, intuitively, one joint interacts differently with various other joints. Hence, MV-IGNet learns diverse patterns for different joint pairs to represent complex actions.

(2) Group-level (group) view divides the skeleton into six parts and draws relationships between the groups. Current graph-based approaches directly aggregate features of all joints to produce final spatial features. This ignores leveraging different granularities of a skeleton. MV-IGNet hierarchically captures spatial features via aggregating and pooling to generate more abstract and comprehensive features. This fashion enriches the learned features of complex actions.

(3) Graph-level (global) view defines all the pairwise interconnecting paths of joints. In previous works, the skeleton topology is fixed and manually defined. This rigid topology ignores massive interactions between joints. MV-IGNet adaptively produces and leverages a topology based on the given skeleton features to flexibly captures the interacting patterns of joints.

These three views mutually provide complementary information and in conjunction describe and understand actions.

#### 4.5 Partitioning Hierarchical Structures

**Spatial Reasoning:** The spatial reasoning and temporal stack learning (SR-TSL) [40] method consists of two modules. The internal spatial reasoning network explicitly learn the hierarchical structural information in two steps. The architecture is visually shown in Figure 22.

First, the skeleton structure is manually partitioned into different functional parts, corresponding to arms, legs and so on. Then, the model integrally capture each part's information via concatenating all the joints' features and processing them through a shared-weight multi-layer perceptron.

Second, different parts jointly form a fully-connected graph and pairwise exchange information to update their features. The authors denote the received information of node  $k$  from node  $i$  at time step  $t$  as  $\mathbf{m}_{ik}^t$ , where  $i \in \{1, \dots, K\}$  and  $K$  is the number of parts. The received information  $\mathbf{m}_k^t$  of node  $k$  from all the neighbors  $\Omega_{v_k}$  at time  $t$  is formulated as:

$$\begin{aligned}\mathbf{m}_k^t &= \sum_{i \in \Omega_{v_k}} \mathbf{m}_{ik}^t \\ &= \sum_{i \in \Omega_{v_k}} \mathbf{W}_m \mathbf{s}_i^{t-1} + \mathbf{b}_m,\end{aligned}\quad (11)$$

where  $\mathbf{s}_i^{t-1}$  stands for the state of node  $i$  at time step  $t-1$ , weights  $\mathbf{W}_m$  and biases  $\mathbf{b}_m$  are trainable. The updates of state  $\mathbf{s}$  and representation  $\mathbf{r}$  can be expressed as:

$$\mathbf{s}_k^t = f_{\text{lstm}}(\mathbf{r}_k^{t-1}, \mathbf{m}_k^t, \mathbf{s}_k^{t-1}), \quad (12)$$

and

$$\mathbf{r}_k^t = \mathbf{r}_k^{t-1} + \mathbf{s}_k^t, \quad (13)$$

where  $f_{\text{lstm}}$  represents the LSTM cell function.

Finally, all the parts' features are concatenated and fed into a multi-layer perceptron to collaboratively produce the latent representation of a temporal frame, formulated as:

$$\mathbf{r}^T = \text{concat}([\mathbf{r}_1^T, \mathbf{r}_2^T, \dots, \mathbf{r}_K^T]), \forall k \in K, \quad (14)$$

$$\mathbf{q} = f_r(\mathbf{r}^T), \quad (15)$$

where  $f_r(\cdot)$  represents a linear layer.

**Two Stream RNN:** The two stream recurrent neural network [39] separately use two parallel branches to integrally capture both temporal and spatial information of skeleton action sequences. The two predictions are finally fused to form the eventual outcome. The visual overall pipeline is shown in Figure 23. We in turn describe the temporal RNN and spatial RNN in the following.

**Temporal RNN:** The temporal RNN comprises of two types: the stacked RNN and the hierarchical RNN. The stacked RNN simply concatenates the coordinates of all joints at each time step. The hierarchical RNN divides the human skeleton into five functional parts: one trunk, two arms and two legs. Then each part is independently processed by an individual RNN. Afterward, all the outputs from every pathway are integrally combined for the final prediction. Figure 24 exhibits the architecture of the hierarchical RNN.

**Spatial RNN:** The spatial RNN sequentially process joint features instead of frame representations. The joint features are orders with two schemes, namely the chain sequence and the traversal sequence. The chain sequence retains the physical connections of the skeleton. The traversal one visits the joint in line with the inherent adjacency relationship.

#### 4.6 P-LSTM

The part-aware long short-term memory (P-LSTM) applies an LSTM to model the skeleton action sequence. Within each unit, a human skeleton is partitioned into five part groups: torso, two hands, and two legs.

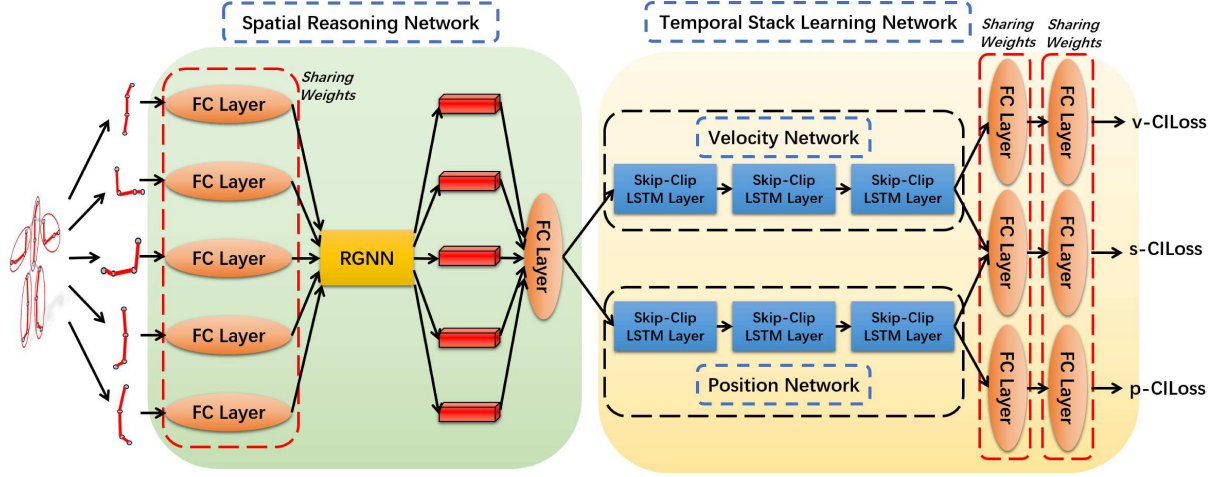


Fig. 22: The architecture of SR-TSL [40]. The left spatial reasoning network spatially extracts hierarchical structural features between different body parts using a residual graph neural network (RGNN). The right temporal stack learning network captures the dynamic characteristics of sequences using two parallel branches. Different loss functions are employed to efficiently train the model. The image is from [40].

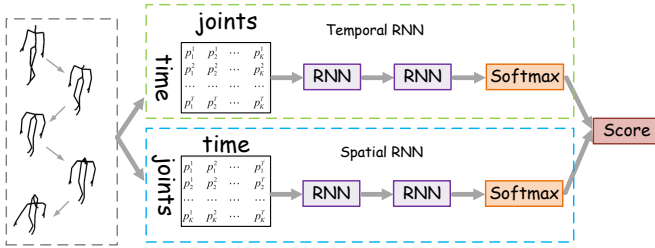


Fig. 23: The overall pipeline of the two-stream RNN for skeleton based action recognition. The image is from [39].

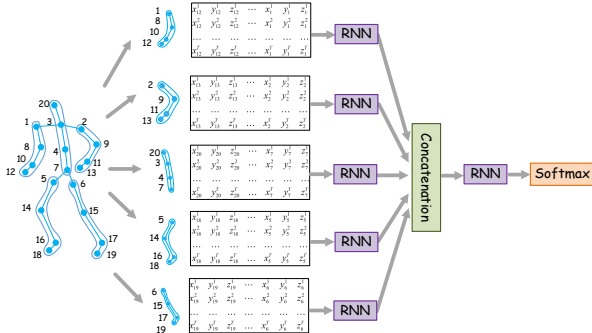


Fig. 24: The architecture of the hierarchical RNN. The image is from [39].

Each part's joint coordinates are concatenated and fed to a unit. That is, before the final operation, different parts' features are independently processed by distinct units. Then, the processed features are concatenated and fused with the representation of the hidden pathway in the form of an elementwise dot product.

**HRNN:** The concept of the hierarchical recurrent neural network (HRNN) proposed in [38] is pictorially depicted in Figure 25. It manually decomposes a human skeleton into five parts. Each is processed by a bidirectional recurrent neural network (BRNN) [63]. As the network layers

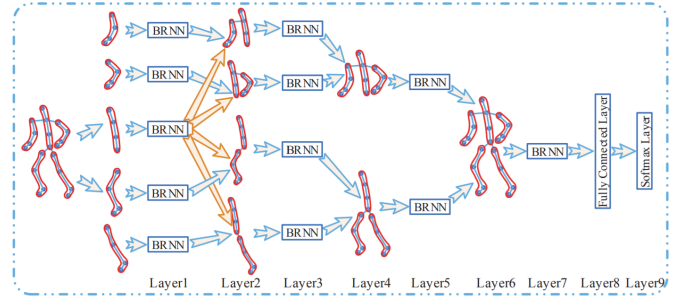


Fig. 25: Conceptual demonstration of the HRNN [38]. BRNN means bidirectional recurrent neural network. The image is from [38].

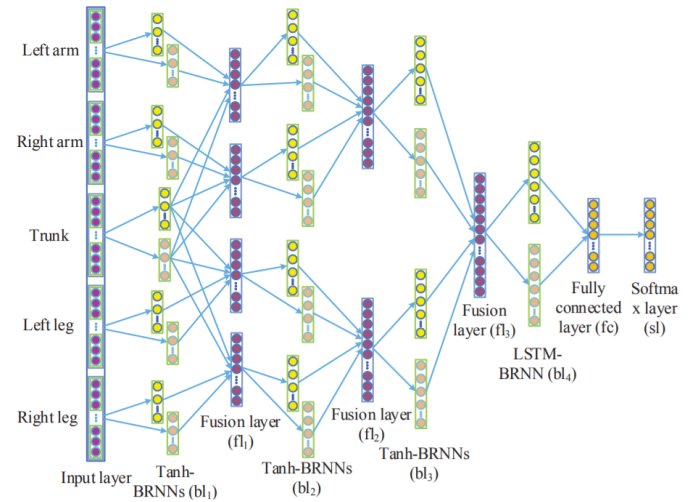


Fig. 26: Architecture illustration of the HRNN [38]. The image is from [38].



go deeper, features of different decomposed components pairwise fuse according to predefined routes to cover more human components. Finally, the resultant feature fully captures information about the entire body. This feature is further transformed by an MLP, followed by the softmax layer to predict the input action. The network is trained with cross-entropy and optimized by the back-propagation through time (BPTT) algorithm [64] as well as the SGD.

The concrete architecture is visually displayed in Figure 26. A human skeleton is decomposed into five non-overlapping parts: left arm, right arm, trunk, left leg, and right leg. In the first layer, features of the four limbs respectively combine with information about the trunk. Then, information within the upper and lower parts of the body separately fuses. That is, communications happen between the features of left and right arms, as well as those of left and right legs. Finally, features from all parts get completely mixed to result in information about the entire body. During this process, feature fusion is implemented with the concatenation operator.

## 5 CAPTURING TEMPORAL PATTERNS

### 5.1 Extracting Multiscale Features

**TS-LSTM:** In [49], the authors propose to additionally use the difference of features between two proximate frames, apart from utilizing the original coordinates. The frame gap between two frames is manually set as a hyperparameter. The authors think this new representation more sufficiently captures the movement patterns. The authors also present the temporal sliding long short-term memory (TS-LSTM) network that jointly capture the short, medium and long temporal features. The predicted results from different features are finally ensembled to further boost accuracy.

### 5.2 Designing Temporal Operators

**G3D:** In [25], as conceptually depicted in the (b) part of Figure 2, the authors propose G3D, a unified convolutional operator that directly models cross-spacetime joint interconnections. G3D integrates neighbor information from not just one single frame, but also from previous and future consecutive frames, resulting in powerful spatial-temporal feature extractors. The entire architecture is visually demonstrated in Figure 27.

**Temporal Stack:** The spatial reasoning and temporal stack learning (SR-TSL) [40] captures temporal dynamics with its temporal stack learning network. The key idea is the internal skip-clip LSTM layer, visually depicted as the temporal stack learning network part of Figure 22 and Figure 28. The entire sequence is uniformly partitioned into  $M$  clips. Each clip independently process its inner frames with a shared LSTM layer. For example, processing the hidden state for the  $m$ -th clip is expressed as:

$$\begin{aligned} \mathbf{h}'_m &= f_{\text{LSTM}}(Q_m) \\ &= f_{\text{LSTM}}(\{\mathbf{q}_{md+1}, \mathbf{q}_{md+2}, \dots, \mathbf{q}_{(m+1)d}\}). \end{aligned} \quad (16)$$

The representation of clip is formulated as:

$$\begin{aligned} \mathbf{H}_m &= \mathbf{H}_{m-1} + \mathbf{h}'_m \\ &= \sum_{i=1}^m \mathbf{h}'_i. \end{aligned} \quad (17)$$

For the input  $\mathbf{x}_t^l$ , it additionally incorporate the previous sequence's information, formulated as the following:

$$\mathbf{x}_t^l = \text{concat}(\mathbf{h}_{t-1}^{l-1}, \mathbf{h}_t^{l-1}). \quad (18)$$

### 5.3 Selecting Informative Frames

**DPRL:** The deep progressive reinforcement learning (DPRL) [52] leverages reinforcement learning to progressively select the most informative frames of a skeleton action sequence. The overview pipeline is illustrated in Figure 29. It includes two sub-networks: frame distillation network (FDNet) and graph-based convolutional network (GCNN). Since the FDNet is the essential part for adaptively selecting discriminative frames, we here primarily concentrate on the FDNet. The GCNN module is utilized to subsequently process and predict the action. The functionality of these two components are visually depicted in Figure 30.

The FDNet formulates the selection of key frames as a Markov decision process (MDP). Its architecture is visually illustrated in Figure 31. We separately elaborate its states, actions and rewards.

**States:** The state consists of two parts  $\{S_a, S_b\}$ . The first part  $S_a$  incorporates the original actional sequence tensor  $F \in \mathbb{R}^{f \times N \times 3}$ , where  $f$  is the number of frames, as well as the tensor corresponding to the selected frames  $M \in \mathbb{R}^{m \times N \times 3}$ , where  $m$  is the number of the selected frames. The second part  $S_b$  is the binary mask of the selected indices. The inclusion of this mask is to let the FDNet explicitly be aware of the selection.

**Actions:** The action is the adjustment direction of each selected frame. There are three types of actions:

- 1) shifting to left,
- 2) staying the same,
- 3) shifting to right.

**Rewards:** The reward is denoted as function  $r(S, A)$ , quantitatively reflecting the quality of an action  $A$  given a state  $S$ . The reward function is produced by the GCNN, formulated as:

$$r_0 = \text{sgn}(P_{n,c} - P_{n-1,c}),$$

where  $c$  represents the ground-truth label, and  $P_{n,c}$  is the probability of predicting the video as label  $c$  at the  $n$ -th iteration. The  $\text{sgn}$  function is applied to more strongly encourage the model to correct wrong predictions.

**GCA-LSTM:** The global context-aware attention LSTM (GCA-LSTM) [51] proactively pays more attention to the more informative frames. To this end, the proposed model consists of two LSTM components. The architecture as well as the pipeline are visually depicted in Figure 32 and Figure 33. The first part is designed to extract global context information of the entire action sequence.

This all-encompassing information is subsequently utilized in conjunction with each separate frame feature to

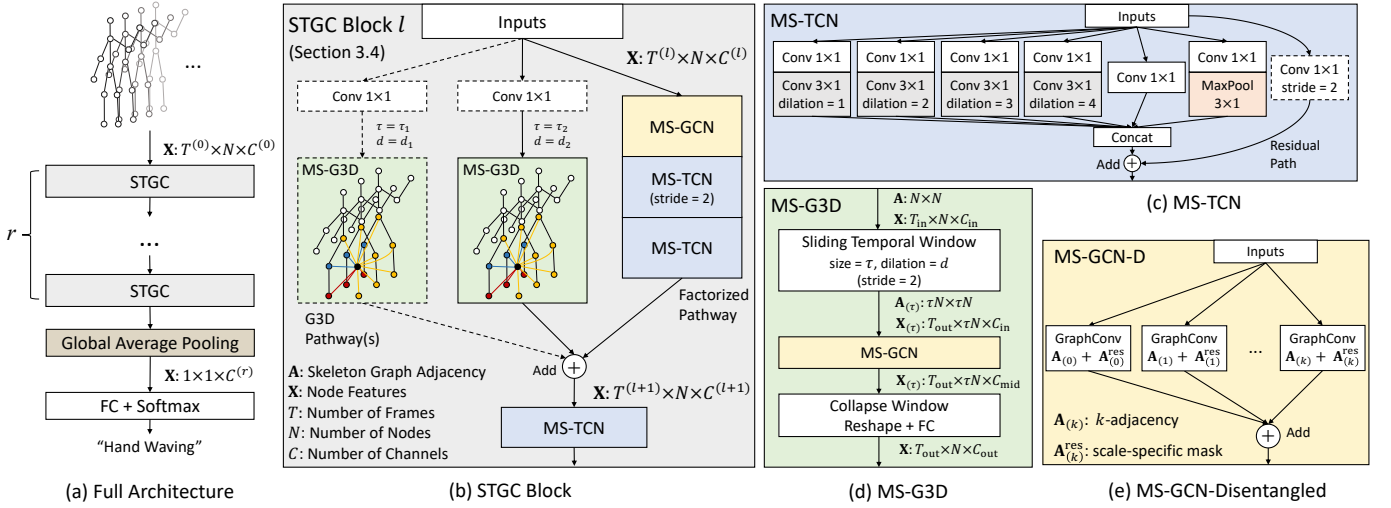


Fig. 27: Illustration of the MS-G3D's architecture. The image is from [25].

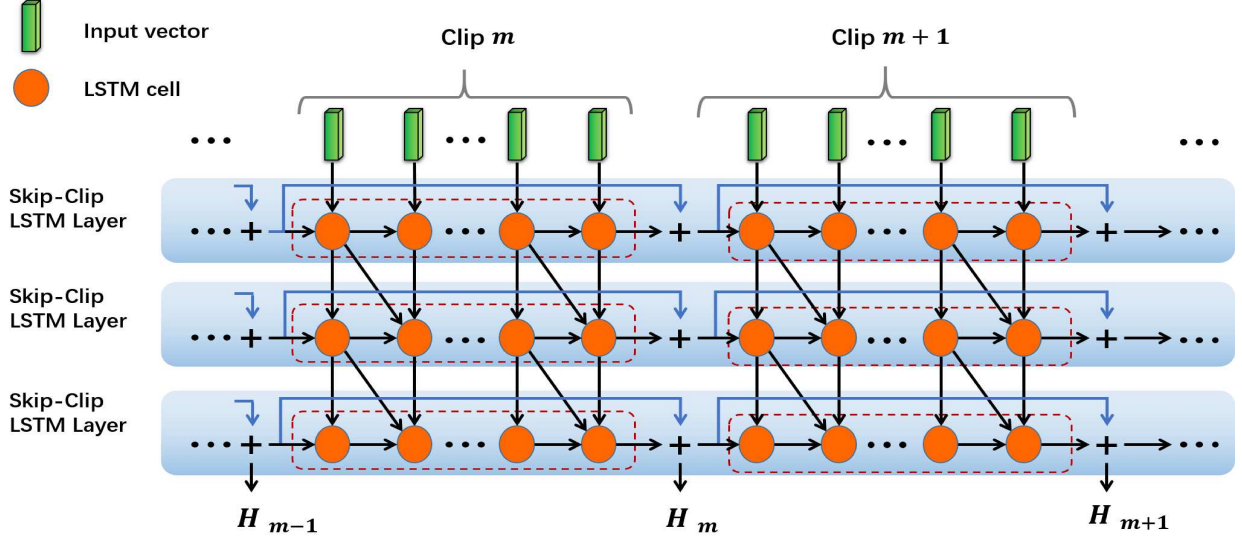


Fig. 28: The architecture of three skip-clip LSTM layers. The image is from [40].

quantitatively assess every frame's importance. The numerical concentration on each frame is further normalized with softmax. Once the model has completed measuring every frame's importance, the global information representation undergoes updating.

## 6 IMPROVING SIGNAL QUALITY

### 6.1 Encoding Semantic Information

**SGN:** In [53], the authors indicate that previous methods may have overlooked the type information of each skeleton joint, and the relative order of frames. [53] proposes a simple yet effective semantics-guided neural network (SGN) for skeleton-based action recognition. The authors enrich the joint feature by explicitly putting in the information of joint types. This information is in the form of one-hot vectors, where the dimension whose value is 1 describes a particular joint type. Similarly, different indices frames are also represented as distinct one-hot vectors.

### 6.2 Transforming Geometric Coordinates

**3D Transformations of Skeletons:** The two stream recurrent neural network [39] additionally augments the original skeleton with their various geometric transformations, including rotation, scaling and shear. The rotation matrices for the  $x$ ,  $y$ , and  $z$  coordinates are formatted as:

$$R_x(\alpha) = \begin{bmatrix} 1 & 0 & 0 \\ 0 & \cos \alpha & -\sin \alpha \\ 0 & \sin \alpha & \cos \alpha \end{bmatrix},$$

$$R_y(\beta) = \begin{bmatrix} \cos \beta & 0 & \sin \beta \\ 0 & 1 & 0 \\ -\sin \beta & 0 & \cos \beta \end{bmatrix},$$

$$R_z(\gamma) = \begin{bmatrix} \cos \gamma & -\sin \gamma & 0 \\ \sin \gamma & \cos \gamma & 0 \\ 0 & 0 & 1 \end{bmatrix}. \quad (19)$$

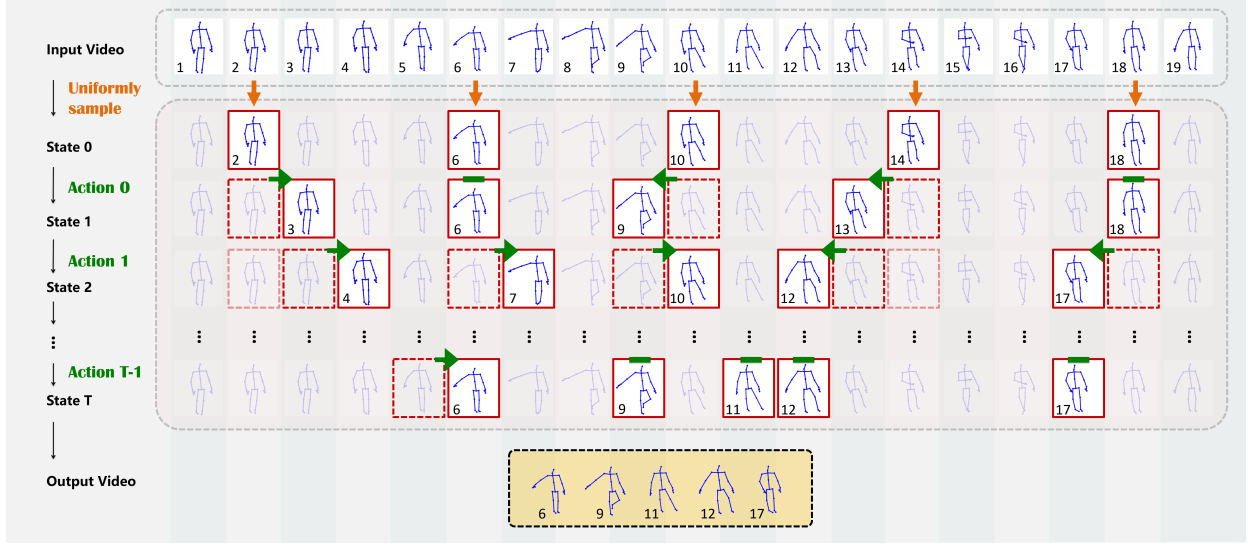


Fig. 29: The overall pipeline of deep progressive reinforcement learning (DPRL) [52]. The input is a skeleton action sequence. The model first uniformly sample several frames. Then, the selection gets progressively adjusted as a Markov decision process. Each state records the original and the selected frames. The actions include ‘shifting to left’, ‘staying the same’ and ‘shifting to right’ for each selected frame. The image is from [52].

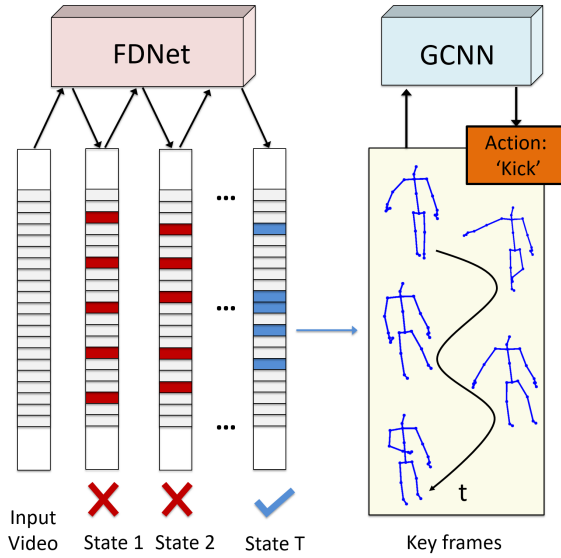


Fig. 30: Visual description of the overall pipeline of deep progressive reinforcement learning (DPRL) [52]. The image is from [52].

The scaling matrix is defined as:

$$S = \begin{bmatrix} s_x & 0 & 0 \\ 0 & s_y & 0 \\ 0 & 0 & s_z \end{bmatrix}. \quad (20)$$

where the scaling factors for the three axes are  $s_x, s_y, s_z$  respectively.

The matrix for shear transformation is defined as:

$$Sh = \begin{bmatrix} 1 & sh_x^y & sh_x^z \\ sh_y^x & 1 & sh_y^z \\ sh_z^x & sh_z^y & 1 \end{bmatrix} \quad (21)$$

where  $sh_x^y, sh_x^z, sh_y^x, sh_y^z, sh_z^x, sh_z^y$  are shear factors.

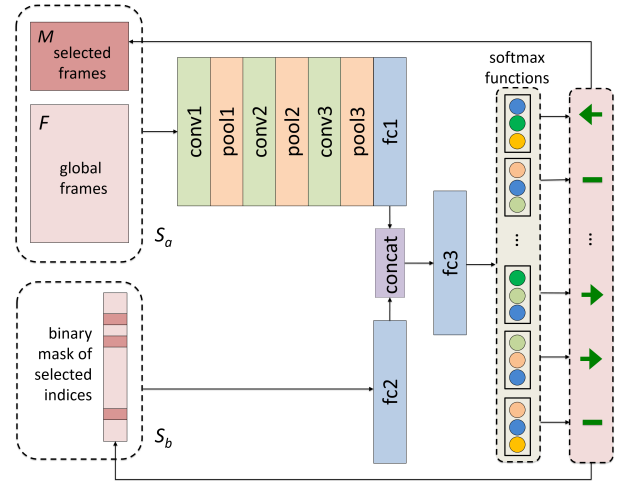


Fig. 31: Architecture illustration of FDNet [52]. The image is from [52].

**Human Cognitive Coordinate Representation:** In [49], the authors propose to geometrically transform the coordinate system of skeletons into a human cognitive coordinate system. In this way, skeletons have the consistent orientation.

**VA-LSTM:** The view adaptive recurrent neural network (VA-RNN) proposed in [14] incorporates two view adaptive subroutine components to geometrically transform different skeletons to be of the same view. They respectively rotate and translate the skeletons to facilitate better recognition.

The implementation details are outlined as follows. In a coordinate system, rotation and translation corresponds to multiplying with a rotation matrix and adding with a vector respectively, as shown in Figure 35. Given dimension  $\beta$ , the

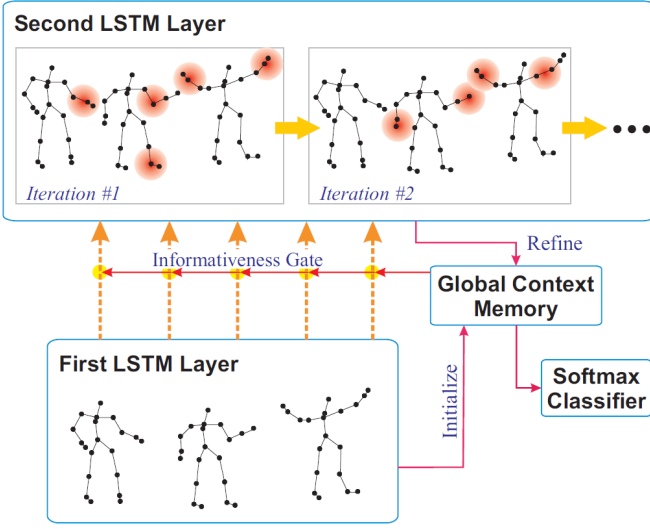


Fig. 32: The visual architecture of the GCA-LSTM. The image is from [51].

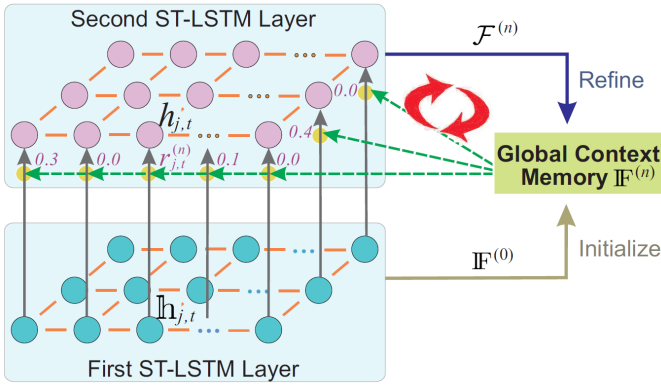


Fig. 33: The visual pipeline of the GCA-LSTM. The image is from [51].

rotation matrix's exact formula is:

$$\mathbf{R}_{t,\beta}^y = \begin{bmatrix} \cos(\beta_t) & \sin(\beta_t) & 0 \\ -\sin(\beta_t) & \cos(\beta_t) & 0 \\ 0 & 0 & 1 \end{bmatrix}. \quad (22)$$

Given a 3D coordinate of dimensions  $\alpha, \beta, \gamma$ , Equation 22 also applies to other two dimensions  $\alpha$  and  $\gamma$ . Therefore, the rotation subnetwork is explicitly to learn the three parameters  $\alpha, \beta, \gamma$ , formulated as:

$$[\alpha_t, \beta_t, \gamma_t]^T = \mathbf{W}_r \mathbf{h}_t^r + \mathbf{b}_r, \quad (23)$$

where  $t$  denotes a frame index,  $\mathbf{h}_t^r$  is a hidden representation of an LSTM layer, and  $\mathbf{W}_r$  is the learned parameter. Similarly, the translation's subnetwork formulation is:

$$\mathbf{d}_t = \mathbf{W}_d \mathbf{h}_t^d + \mathbf{b}_d. \quad (24)$$

$\mathbf{d}_t$  stands for the magnitude of translating.

The entire architecture is illustrated in Figure 34.

### 6.3 Mitigating Overfitting Problems

**Edge-Drop:** [31] aims to improving the dropout operation on graph representations. The dropout operation has been

shown to robustly improve the model's generalizability. The authors propose a new dropout mechanism specialized for graph neural networks. The key idea is to reduce the unnecessary coupling between joint features. To this end, when dropping a node, its neighbors' features are also along removed. To further enhance the dropout's effectiveness, the features to drop are guided by an attention map. The features with high activation values are more likely to be discarded to more easily induce the model to learn more salient and discriminative features.

## 7 PROPOSING LEARNING FRAMEWORKS

### 7.1 Applying Statistical Frameworks

**Bayesian GC-LSTM:** In [65], the authors propose a Bayesian framework to improve the model's robustness and generalizability. The authors propose an adversarial prior to regularize the model's parameters. The prior distribution of the model parameters is set to be Gaussian. The procedures are visually depicted in [65].

### 7.2 Alleviating Signal Noise

**Trust Gate:** ST-LSTM incorporates the trust gates that are specifically designed to alleviate the adverse influence of noise [19]. The noise can be the wrongly estimated joint coordinates due to occlusion, internal errors and so on.

The idea is derived from the assumption that the features of the next iterative step can be accurately predicted given high-quality previous features. Based on this, the authors utilize the predicted values' accuracy as the reliability of the learned features. If the prediction is poor, the ST-LSTM then assigns low weights to the corresponding features.

The concrete architecture is visually illustrated in Figure 37. The trust gate first predicts value  $p_{j,t}$  at joint  $j$  and time  $t$ :

$$p_{j,t} = \tanh \left( M_p \begin{pmatrix} \mathbf{h}_{j-1,t} \\ \mathbf{h}_{j,t-1} \end{pmatrix} \right), \quad (25)$$

where  $\mathbf{h}_{j-1,t}$  and  $\mathbf{h}_{j,t-1}$  are hidden representations of the previous joint and time,  $M_p$  is the weight. The transformation with the same form but using the features at joint  $j$  and time  $t$  and a different weight  $M_x$  is applied to obtain  $x'_{j,t}$ . Then, the gate evaluates the difference between the values predicted using the previous and true values:

$$\begin{aligned} x'_{j,t} &= \tanh (M_x (x_{j,t})), \\ \tau_{j,t} &= G(x'_{j,t} - p_{j,t}), \end{aligned} \quad (26)$$

where  $G$  is a monotonically decreasing function defined as:

$$G(z) = \exp(-\lambda z^2), \quad (27)$$

where  $\lambda$  is a hyperparameter. That is, a larger difference leads to a lower value of  $G$ . Finally, the mathematical form of updating the trust gate is:

$$\begin{aligned} c_{j,t} &= \tau_{j,t} \odot i_{j,t} \odot u_{j,t} \\ &+ (1 - \tau_{j,t}) \odot f_{j,t}^S \odot c_{j-1,t} \\ &+ (1 - \tau_{j,t}) \odot f_{j,t}^T \odot c_{j,t-1}. \end{aligned} \quad (28)$$

The formula implies that given more reliable previous values, the ST-LSTM utilizes less historical information in the forgetting gates.



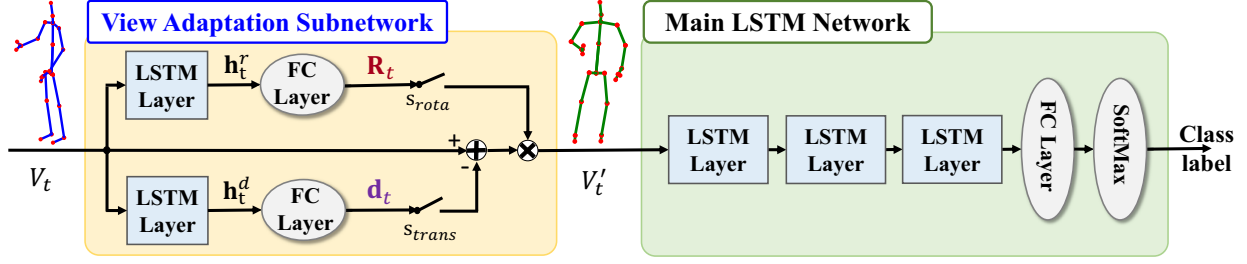


Fig. 34: Illustration of the entire architecture. The skeleton is first geometrically transformed via rotation and translation. Then, the re-positioned skeleton is subsequently fed to the main LSTM network for action recognition. This image is from [14].

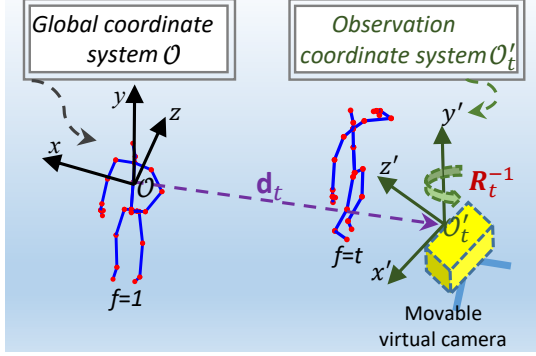


Fig. 35: Illustration of rotating and translating a skeleton. The skeleton is re-positioned via a  $d_t$  translation and a rotation around the X-axis, Y-axis, and Z-axis. This image is from [14].

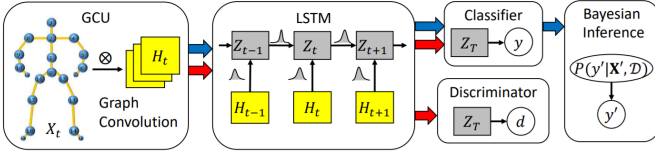


Fig. 36: Illustration of the procedures of [65]. The image is from [65].

## 8 SOTA RESULT IMPROVEMENT

In this section, we display the evaluated results of different approaches on various datasets.

TABLE 1: SOTA result improvement for the Berkeley MHAD dataset [10]. Acc (%) stands for accuracy. # Ens indicates the number of ensembling models.

Methods	# Ens	Acc (%)
HRNN [38]	1	100

TABLE 2: SOTA result improvement for the Motion Capture Dataset HDM05 [5]. Acc (%) stands for the average accuracy. STD means the standard deviation. # Ens indicates the number of ensembling models.

Methods	# Ens	Acc (%)	STD
HRNN [38]	1	96.2	0.5

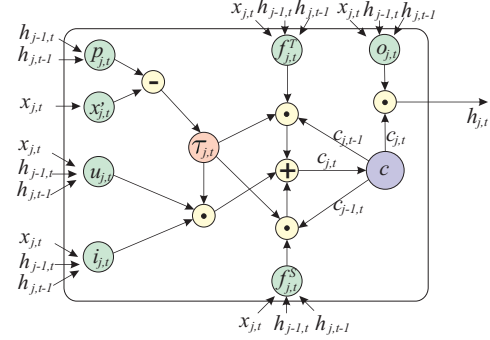


Fig. 37: Architecture of the proposed ST-LSTM [19] with trust gate. The image is from [19].

TABLE 3: SOTA result improvement for the SBU Interaction dataset [7]. Acc (%) stands for accuracy. # Ens indicates the number of ensembling models.

Methods	# Ens	Acc (%)
ST-LSTM [19]	1	93.3
VA-LSTM [14]	1	97.2
Two-Stream RNN [39]	1	90.2
C-CNN [20]	1	93.6

TABLE 4: SOTA result improvement for the UT-Kinect Action3D dataset [7]. Acc (%) stands for accuracy. # Ens indicates the number of ensembling models.

Methods	# Ens	Acc (%)
ST-LSTM [19]	1	97.0
GCA-LSTM [51]	1	98.5
DPRL [52]	1	98.5

TABLE 5: SOTA result improvement for the CMU dataset [7]. Acc (%) stands for accuracy. # Ens indicates the number of ensembling models.

Methods	# Ens	Acc (%)
C-CNN [19]	1	83.3

## 9 ANUBIS: A NEW LARGE-SCALE DATASET

In section 2, we have reviewed various kinds of approaches for skeleton-based action recognition. In this section, we comparably benchmark their performance on a large-scale skeleton dataset that is newly collected by us. Although previously some skeleton datasets have been proposed, the

TABLE 6: SOTA result improvement for the Northwestern UCLA dataset [12]. Acc (%) stands for accuracy. # Ens indicates the number of ensembling models.

Methods	# Ens	Acc (%)
TS-LSTM [49]	1	89.2
AGC-LSTM [28]	1	93.3
Shift-GCN [30]	1	94.6

TABLE 7: SOTA result improvement for the UWA3DII dataset [14]. Acc (%) stands for accuracy. # Ens indicates the number of ensembling models.

Methods	# Ens	Acc (%)
TS-LSTM [49]	1	75.6

TABLE 8: SOTA result improvement for the SYSU 3D Human-Object Interaction dataset [13]. Acc (%) stands for accuracy. # Ens indicates the number of ensembling models. CS and SS correspond to the cross-subject and same-subject settings respectively.

Methods	# Ens	SYSU	
		CS	SS
VA-LSTM [14]	1	77.5	76.9
SR-TSL [40]	1	80.7	81.9
SGN [40]	1	89.3	90.6

TABLE 9: SOTA result improvement for the Kinetics dataset [15]. Acc (%) stands for accuracy. # Ens indicates the number of ensembling models.

Methods	# Ens	Kinetics	
		Top-1	Top-5
DGNN [24]	1	36.9	59.5
2s-AGCN [34]	2	36.1	58.7
AS-GCN [33]	2	34.8	56.5
CA-GCN [35]	2	34.1	56.6
MSG3D [25]	2	38.0	60.9

newly created dataset additionally offers multiple properties that existing datasets do not possess, as described below.

- 1) **More recently released sensors:** We apply several lately unveiled product, Microsoft Azure Kinect cameras (Azure Kinect), as the skeleton extractors. In contrast, existing datasets utilize more dated sensors, such as the predecessors of Azure Kinect, Microsoft Kinect V1 and V2 for NTU60 [11] and NTU120 [16].
- 2) **Novel back view:** We include the skeletons that are captured from the subjects who have their backs toward the cameras. This is a novel capturing perspective that is absent in existing datasets.
- 3) **High enthusiasm of subjects:** We jointly apply numerous strategies to arouse the participants' enthusiasm and expressiveness to ensure the collected skeleton actions are loyal to reality. The adopted strategies are new in comparison with previous methods for collecting skeletons.
- 4) **Actions in the pandemic era:** We incorporate many actions that are common during the pandemic era,

TABLE 10: SOTA result improvement for the NTU datasets.

(a) NTU60. X-Sub and X-View represent the cross-subject and cross-view settings respectively. # Ens indicates the number of ensembling models.

Methods	# Ens	NTU60	
		X-Sub	X-View
P-LSTM [11]	1	62.9	70.3
ST-LSTM [19]	1	69.2	77.7
VA-LSTM [14]	1	79.4	87.6
GCA-LSTM [51]	1	74.4	82.8
C-CNN [20]	1	79.6	84.8
Two-Stream RNN [39]	1	71.3	79.5
TS-LSTM [49]	1	74.6	81.3
DPRL [52]	1	83.5	89.8
SR-TSL [40]	1	84.8	92.4
AGC-LSTM [28]	1	89.2	95.0
AS-GCN [33]	1	86.8	94.2
2s-AGCN [34]	2	88.5	95.1
DGNN [24]	2	89.9	96.1
Bayesian GCN [65]	1	81.8	89.0
MSG3D [25]	2	91.5	96.2
Shift-GCN [30]	2	89.7	96.0
CA-GCN [35]	4	90.7	96.5
SGN [53]	1	89.0	94.5
Decouple-GCN [31]	4	90.8	96.6

(b) NTU120. X-Sub and X-Set represent the cross-subject and cross-setup settings respectively. # Ens indicates the number of ensembling models.

Methods	# Ens	NTU120	
		X-Sub	X-View
P-LSTM [11]	1	25.5	26.3
ST-LSTM [19]	1	55.7	57.9
GCA-LSTM [66]	1	58.3	59.2
2s-AGCN [34]	1	82.9	84.9
Shift-GCN [67]	4	85.9	87.6
MSG3D [25]	2	86.9	88.4
SGN [53]	1	79.2	81.5
DecoupleGCN [31]	4	86.5	88.1

Specification	Value
Num. of Actions	102
Num. of participants	80
Num. of views	80

TABLE 11: Specifications of ANUBIS.

such as elbow touching and fist bumping.

We name the new dataset as ANUBIS, standing for *Australian National University Benchmarking Indoor Skeletons*. Apart from this meaning, Anubis is also the name of an ancient Egyptian god of the dead. We hence believe the name suitably refers to a dataset of skeletons. As a brief overview, we summarize the main specifications of ANUBIS as Table 11.

## 10 COLLECTION PROCESS

We here describe how to strongly arouse participants' motivations, settings of the collecting process, as well as the incorporated actions.

### 10.1 Incentives

Participants' degree of cooperation strongly influences the quality of the collected data. Skeletons with poor quality

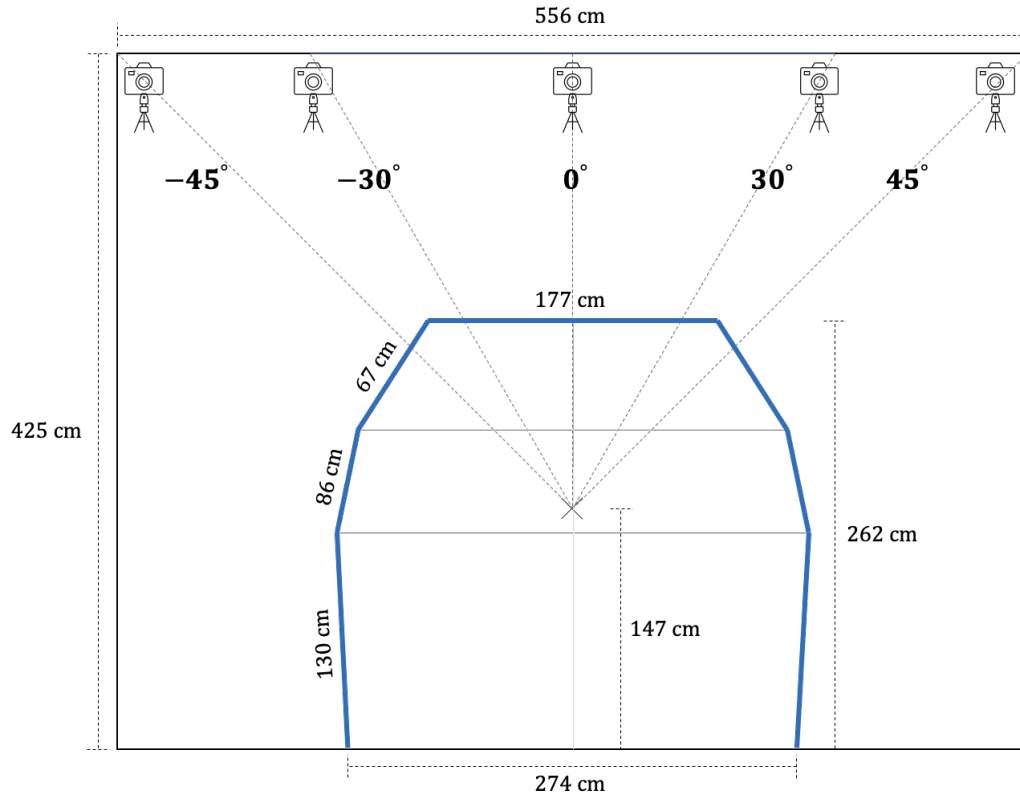


Fig. 38: Illustration of the venue setup for collecting the ANUBIS dataset.



Fig. 39: Illustration of the camera setup for collecting the ANUBIS dataset.

obstruct training an accurate action recognizer as well as causes unreliability of fairly evaluating different models.

During the process of our pilot studies, we observe some unenthusiastic participants. They lazily perform tiny movements for almost all actions, resulting the motion trajectories of different actions to be unexpectedly similar. Some people even wrongly conduct actions. For example, they do exactly the same movements for both front-kicking and side-kicking. These people also persistently refused to correct their behaviors.

We aim to maximally arouse the participants' enthusiasm to ensure the high-quality of the collected data. To this end, we follow the following three strategies for all the participants:

- 1) **Our great service enthusiasm:** All experimenters endeavor presenting the utmost service to the participants in order to let them feel that they are warmly treated.
- 2) **Free food and snacks:** We provide the participants with free buffet-like snacks and drinks. We neatly exhibit them on a table. Participants can freely pick and consume. For people who are shy and refuse the treatment, we will actively put some on their hands as ice breaking.
- 3) **Physical strength preservation:** Participants can ask for a break at any time. During the break time, we will warmly bring chairs to them and feed them with snacks and drinks. For those who have been continuously performing without any rest, we will proactively interrupt the session to let them take a break.

Additionally, many students are required to participants data collection sessions to get necessary credits for graduation. As experimenters, we have the rights to not grant credits for unenthusiastic subjects.

For poorly performed actions, we will discard the corresponding data.

## 10.2 Collection Setups

We setup the skeleton collection venue as visually described in Figure 38. The camera setup in the room is as Figure 39. We place five Azure Kinect devices in the front of the room facing to the other side. For these five devices, one is located in the middle, straightly facing toward the subjects. The other four cameras are established at the two sides of the middle line, forming two symmetric pairs. The two pairs of devices face toward the subjects with  $\pm 30$  and  $\pm 45$  degrees.

Two participants involve in each collection session. They perform either interactive or independent actions. Interactive actions require two participants simultaneous behaviors, such as shaking hands and exchange objects. Independent actions are two non-related actions performed by two distinct persons, such as drinking water and standing up.

The pair of participants conduct the same action four times. During each time, every individual subject acts differently, resulting in four different variations:

- 1) The participants perform the instructed action facing to the camera.

- 2) The two persons turn their back to the cameras and do the same action.
- 3) The two subjects turn around to face to the cameras again and switch the standing positions. For an interactive action, the two subjects also exchange the active and passive relationships. For example, within a kicking action, the kicking person then becomes the one who is kicked, and the one being kicked starts acting kicking.
- 4) The two people turn their back to the cameras while sticking to the current standing positions and perform the action again.

## 10.3 Encouraging Superb Acting

We desire the performed actions to be similar to the ones happening in the real life. However, this desirability is unrealistic for many actions, particularly for the ones mimicking violent behaviors. One example can be *pulling hair*. On the one hand, it is unethically infeasible to request one person to actually pull the other performer's hair; on the other hand, we aspire the actors to conduct lively performances that are close to reality. That is, a dilemma exists between the loyalty to the reality and the ethics of the subjects.

To bypass the dilemma, we leverage different acting tools, including toy knives, toy guns, and many more. For example, to tackle the above example *pulling hair*, we provide the performers with a wig to prevent physical harm to the person meanwhile also maximize the loyalty to the real scenarios. As for the other actions that result in the identical dilemma, we list their corresponding performing tools and the descriptions that how the tools address the dilemma in the list below.

- **cover mouth:** we apply tissues to prevent the physical contact between one's hand and the other's mouth.
- **hit with object:** we utilize a light paper box to prevent the harm to the person when hitting.
- **use cigarette to burn:** we use a unlit cigarette to encourage more close-to-reality performances.
- **pick and throw an object to person:** we employ an extremely light paper ball to promote more expressive performances.
- **shoot person:** we let the performer operate a toy gun to facilitate more lively actions.
- **wave knife to others & cut person & self-cutting with knife:** we provide the actors with a toy dagger to boost their empathy.

Apart from the actions involving the dilemma, we also offer the participants various tools for other actions to arouse their sense of immersion, including backpacks, cups, and creams. From our observations, the participants enjoyed their acting and presented expressive performances.

## 10.4 Action List

The incorporated actions are listed in the following list, sorted by interactive or non-interactive ones. We also encompass COVID-related actions in accordance with the current world trend.



- 1) **Interactive:** rock-paper-scissors, touch elbows, fist bumping, pat on shoulders, giving object, exchange object, shake hands, whisper, clapping each other, walk apart, walk form apart to together, cheers and drink, hit with knees, hit with head, support with arms to help old people walking, punch to face, punch to body, cover mouth, strangling neck, slap, kicking, pushing, pierce arms, pull hairs, drag other person (other resist), pull collar, shake others, beat with elbow, knock over, hit with object, point to person, lift ear, pinch arms, use cigarette to burn, sidekick person, pick and throw an object to person, shoot person, stab person, wave knife to others, splash liquid on person, stumble person, step on foot, pickpocketing, bite person, take picture for others (sneakily), spiting to person, chop (cut) person, take chair while other sitting, hit the head with hand, pinch face with two hands, pinch body (not arm), follow person, belt person.
- 2) **Independent:** nod head, bow, wave hand, clapping, hushing, drink water, brush teeth, stand up, jump up, take off a hat, play a phone, take a selfie, wipe face, cross hands in front, throat-slitting, crawling, open bottle, sneeze, yawn, self-cutting with knife, take off headphone, stretch oneself, flick hair, thumb up, thumb down, make ok sign, make victory sign, cutting nails, cutting paper, squat down, toss a coin, fold paper, ball up paper, play magic cube, surrender, apply cream on face, apply cream on hand, put on bag, take off bag, put object into bag, take object out of bag, open a box, yelling, arm circles, arm swings, running, vomiting, headache, back pain, falling down, chest pain.

## 10.5 Evaluation

We utilize our collected dataset for benchmarking existing approaches for skeleton-based action recognition.

We employ PyTorch as the framework and are train the models on one NVIDIA 3090 GPU for 50 epochs. We apply stochastic gradient descent (SGD) with momentum 0.9 as the optimizer. The learning rate is set as 0.05 at the beginning and decays to be 10% at epoch 30. Following [24], we preprocess the skeleton data with normalization and translation, padding each video clip to be of the same length of 300 frames by repeating the actions.

The benchmarking results on ANUBIS are reported in Table 12. We not only include the top-1 and top-5 accuracy values for fairly assessing the classification performance of each approach, but we also incorporate every model’s size and operational times measured by number of parameters and giga flops respectively.

We further ensemble the evaluated methods together and analyze the confusion matrix of the ensembled performance for skeleton-based action recognition.

## 11 CONCLUSION AND FUTURE WORK

We have reviewed a variety of approaches for skeleton-based action recognition, a human-centered computer vision problem that is swiftly accumulating attention. We have

TABLE 12: Results of benchmarking existing methods for skeleton-based action recognition on ANUBIS. We include the top-1 and top-5 accuracy as well as the total number of parameters (#params) and inference time (GFlops) in the networks.

Methods	Top-1 Acc (%)	Top-5 Acc (%)	# Params (M)	GFlops
STGCN [61]	50.25	79.96	3.4	45.18
Motif-STGCN [26]	55.76	83.96	1.78	27.10
Dual-AGCN [34]	57.26	84.86	3.47	47.84
RA-GCN [27]	41.87	73.45	10.26	135.52
MS-G3D [25]	54.17	82.05	3.80	62.72
Shift-GCN [30]	26.84	57.50	0.73	6.16
Decouple-GCN [31]	52.32	80.06	3.63	32.98
GCN-NAS [48]	56.40	84.37	6.57	93.64
CTR-GCN [32]	37.90	70.40	10.07	141.68

TABLE 13: The 20 lowest-accurate actions of ANUBIS.

Action	Acc (%)	Most Confusing Action
fold paper	4.35	cutting nails
take object out of bag	4.85	self-cutting with knife
make victory sign	8.77	make ok sign
play magic cube	9.94	cutting nails
flick hair	10.27	sneeze
cutting paper	13.06	cutting nails
open bottle	14.16	open bottle
take off headphone	16.31	take off headphone
surrender	19.87	surrender
wipe face	20.06	yawn
ball up paper	21.12	ball up paper
make ok sign	21.75	make ok sign
pinch arms	22.94	pinch body (not arm)
put object into bag	22.98	self-cutting with knife
brush teeth	23.42	drink water
chop (cut) person	25.08	hit with object
hit the head with hand	25.67	hit with object
self-cutting with knife	26.89	cutting nails
pinch face with two hands	26.95	strangling neck
apply cream on hand	27.42	play a phone

TABLE 14: The 20 highest-accurate actions of ANUBIS.

Action	Acc (%)	Most Confusing Action
walk apart	97.09	follow person
clapping each other	96.44	exchange object
bow	91.12	hit with head
nod head	90.94	take picture for others (sneakily)
cheers and drink	90.23	giving object
walk form apart to together	89.94	follow person
clapping and hushing	89.29	wave hand
rock-paper-scissors	87.57	shake hands
knock over	86.11	take chair while other sitting
squat down	83.33	toss a coin
whisper	82.52	hit with head
exchange object	81.93	giving object
arm circles	81.23	arm swings
pushing	79.32	punch to body
wave hand	78.40	clapping and hushing
shake hands	78.30	giving object
falling down	78.29	chest pain
take chair while other sitting	76.85	knock over
shoot person	75.41	take picture for others (sneakily)
cross hands in front	75.22	throat-slitting

also created a large-scale human skeleton dataset, on which we have evaluated numerous methods. In this section, we expect extensive thriving directions to appear in the near future. Here, we list several directions that may not have been fully saturated. We also propose a few new problems that we think are necessary to solve in order to commercialize

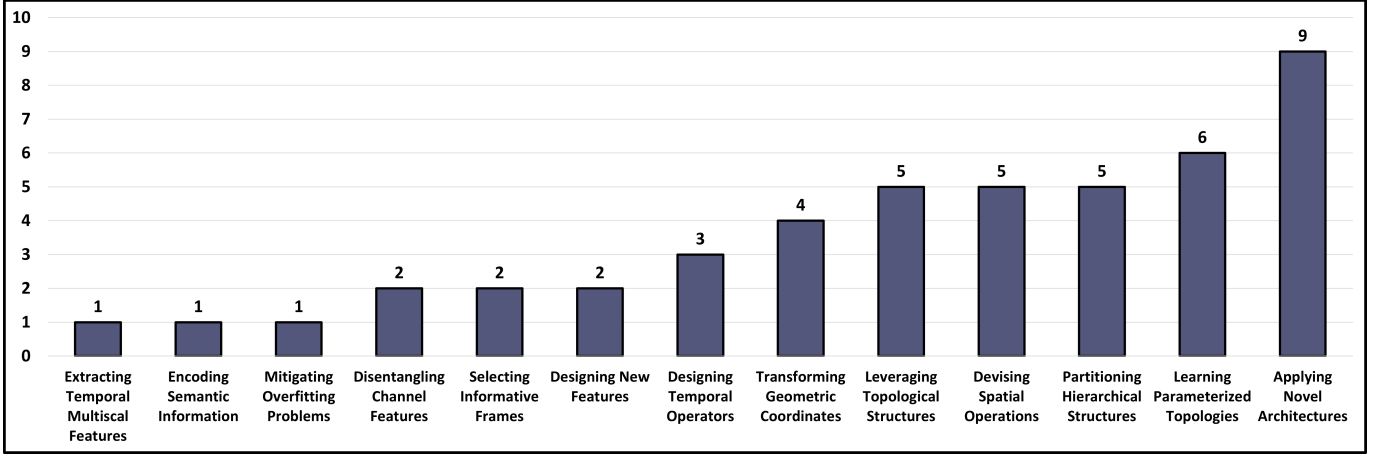


Fig. 40: Proportions of the functional categories of literature on skeleton-based action recognition. Sorted smaller to larger from left to right.

skeleton-based action recognition in real-world scenarios.

## 11.1 Future Directions

In the literature review part of skeleton-based action recognition, we divide existing methods into 13 categories except the dataset one according to how do they functionally tackle the problem. Here, we further count each category's proportion and thereby sort the classes. The results are visually shown in Figure 40. Note that a single paper can simultaneously belong to multiple functional groups.

We observe that the majority of literature concentrates on applying novel architectures and learning parameterized topologies. Both these two groups focus on more adequately extracting structural information.

On the flip side, from these statistics, we consider the following directions below are relatively rarely investigated: (1) properly utilizing multiscale temporal features, (2) more elegantly encoding semantic information, and (3) better mitigating overfitting.

## 11.2 Future Problems

### 11.2.1 Retrieval between Skeleton and RGB Data

To ensure the protection of personal privacy, RGB videos may be separately stored in another place different from that of skeleton data. On the other hand, usage of RGB data is inevitable in some situations. For example, to undoubtedly convict a person to be guilty, the presence of the person's RGB videos containing crime activities with clear identity information is indispensable.

This brings the need of retrieving the corresponding RGB videos with the skeleton sequences as the index. To illustrate, in a school, skeleton sequences evidently indicate violent behaviors have happened. We subsequently demand to exactly identify the perpetrators and victims. The school administrators hence then need to obtain the corresponding RGB videos from the authority. Manually fetching the corresponding RGB video from the skeleton one is laborious. It is ideal if the machine can automatically conduct the fetching.

### 11.2.2 Individual Action Recognition in Groups

The current setting of the skeleton-based action recognition problem assumes that each skeleton sequence merely contains a single action. In contrast, a randomly captured skeleton video is likely to include more than one action. Hence, in a more realistic scenario, we are required to elegantly solve the following two problems:

- 1) Recognizing each individual's action.
- 2) Detecting who is performing in conjunction with whom.

The conjunction of these two problems jointly forms the new problem of individual action recognition in groups.

### 11.2.3 Skeleton-Based Temporal Action Detection

This problem involves identifying the starting and ending frames of an action given a long skeleton sequence internally containing multiple actions. Meanwhile, we predict the action label for each extracted subsequence.

The collection protocol of the ANUBIS dataset intrinsically grants defining this problem. When collecting the human skeletons, we let the Kinect devices keep recording throughout the entire collection session. Meanwhile, we recorded the starting and ending timestamps of each action. Each action's skeleton sequence is subsequently trimmed out according to these timestamp marks. Hence, when defining this problem, we can use the whole untrimmed video as the input data. The recorded starting and ending timestamps will serve as ground-truth information.

### 11.2.4 Skeleton-Based Action Anticipation

In future, robots may work closely with humans. If an action that is about to happen or is at an early stage, such as people falling or fighting, we wish robots' immediate intervene. Thus, we aim to recognize actions in an online fashion. Inspired by this, the problem is described as that given a new frame, we aim to accurately recognize the action that is happening, even the action has not completed.

## REFERENCES

- [1] T. U. Nations. (2019) World population aging. [Online]. Available: <https://www.un.org/en/development/desa/population/> 1
- [2] G. Newswire. (2021) Virtual reality (vr) market to reach usd 84.09 billion by 2028. [Online]. Available: <https://www.globenewswire.com/> 1
- [3] Markets and Markets. (2021) Video surveillance market with covid-19 impact analysis, by offering. [Online]. Available: <https://www.marketsandmarkets.com/Market-Reports/video-surveillance-market-645.html> 1
- [4] G. Johansson, "Visual perception of biological motion and a model for its analysis," *Perception & psychophysics*, vol. 14, no. 2, pp. 201–211, 1973. 2
- [5] M. Müller, T. Röder, M. Clausen, B. Eberhardt, B. Krüger, and A. Weber, "Documentation mocap database hdm05," 2007. 3, 17
- [6] W. Li, Z. Zhang, and Z. Liu, "Action recognition based on a bag of 3d points," in *2010 IEEE Computer Society Conference on Computer Vision and Pattern Recognition-Workshops*. IEEE, 2010, pp. 9–14. 3
- [7] K. Yun, J. Honorio, D. Chattopadhyay, T. L. Berg, and D. Samaras, "Two-person interaction detection using body-pose features and multiple instance learning," in *2012 IEEE Computer Society Conference on Computer Vision and Pattern Recognition Workshops*. IEEE, 2012, pp. 28–35. 3, 17
- [8] L. Xia, C.-C. Chen, and J. K. Aggarwal, "View invariant human action recognition using histograms of 3d joints," in *2012 IEEE computer society conference on computer vision and pattern recognition workshops*. IEEE, 2012, pp. 20–27. 3
- [9] CMU. (2012) Cmu graphics lab motion capture database. [Online]. Available: <http://mocap.cs.cmu.edu/> 3
- [10] F. Ofli, R. Chaudhry, G. Kurillo, R. Vidal, and R. Bajcsy, "Berkeley mhad: A comprehensive multimodal human action database," in *2013 IEEE Workshop on Applications of Computer Vision (WACV)*. IEEE, 2013, pp. 53–60. 3, 17
- [11] A. Shahroudy, J. Liu, T.-T. Ng, and G. Wang, "Ntu rgb+ d: A large scale dataset for 3d human activity analysis," in *Proceedings of the IEEE conference on computer vision and pattern recognition*, 2016, pp. 1010–1019. 3, 4, 18
- [12] J. Wang. (2015) Northwestern-ucla multiview action 3d dataset. [Online]. Available: [https://wangjiangb.github.io/my\\_data.html](https://wangjiangb.github.io/my_data.html) 3, 18
- [13] J.-F. Hu, W.-S. Zheng, J. Lai, and J. Zhang, "Jointly learning heterogeneous features for rgb-d activity recognition," in *Proceedings of the IEEE conference on computer vision and pattern recognition*, 2015, pp. 5344–5352. 3, 18
- [14] P. Zhang, C. Lan, J. Xing, W. Zeng, J. Xue, and N. Zheng, "View adaptive recurrent neural networks for high performance human action recognition from skeleton data," in *Proceedings of the IEEE International Conference on Computer Vision*, 2017, pp. 2117–2126. 3, 15, 17, 18
- [15] J. Carreira and A. Zisserman, "Quo vadis, action recognition? a new model and the kinetics dataset," in *IEEE Conference on Computer Vision and Pattern Recognition (CVPR)*, 2017. 3, 18
- [16] J. Liu, A. Shahroudy, M. L. Perez, G. Wang, L.-Y. Duan, and A. K. Chichung, "Ntu rgb+ d 120: A large-scale benchmark for 3d human activity understanding," *IEEE Conference on Computer Vision and Pattern Recognition (T-PAMI)*, 2019. 3, 4, 18
- [17] P. Gupta, A. Thatipelli, A. Aggarwal, S. Maheshwari, N. Trivedi, S. Das, and R. K. Sarvadevabhatla, "Quo vadis, skeleton action recognition?" *International Journal of Computer Vision (IJCV)*, vol. 129, no. 7, pp. 2097–2112, 2021. 3
- [18] M. E. Hussein, M. Torki, M. A. Gowayyed, and M. El-Saban, "Human action recognition using a temporal hierarchy of covariance descriptors on 3d joint locations," in *International Joint Conference on Artificial Intelligence (IJCAI)*, 2013. 3
- [19] J. Liu, A. Shahroudy, D. Xu, and G. Wang, "Spatio-temporal lstm with trust gates for 3d human action recognition," in *European conference on computer vision*. Springer, 2016, pp. 816–833. 3, 5, 6, 16, 17, 18
- [20] Q. Ke, M. Bennamoun, S. An, F. Sohel, and F. Boussaid, "A new representation of skeleton sequences for 3d action recognition," in *Proceedings of the IEEE conference on computer vision and pattern recognition*, 2017, pp. 3288–3297. 3, 4, 5, 6, 17, 18
- [21] T. M. Le, N. Inoue, and K. Shinoda, "A fine-to-coarse convolutional neural network for 3d human action recognition," *The British Machine Vision Conference (BMVC)*, 2018. 3
- [22] K. Thakkar and P. Narayanan, "Part-based graph convolutional network for action recognition," *The British Machine Vision Conference (BMVC)*, 2018. 3
- [23] C. Li, Q. Zhong, D. Xie, and S. Pu, "Co-occurrence feature learning from skeleton data for action recognition and detection with hierarchical aggregation," *International Joint Conference on Artificial Intelligence (IJCAI)*, 2018. 3
- [24] L. Shi, Y. Zhang, J. Cheng, and H. Lu, "Skeleton-based action recognition with directed graph neural networks," in *Proceedings of the IEEE/CVF Conference on Computer Vision and Pattern Recognition*, 2019, pp. 7912–7921. 3, 4, 18, 21
- [25] Z. Liu, H. Zhang, Z. Chen, Z. Wang, and W. Ouyang, "Disentangling and unifying graph convolutions for skeleton-based action recognition," in *Proceedings of the IEEE/CVF conference on computer vision and pattern recognition*, 2020, pp. 143–152. 3, 4, 13, 14, 18, 21
- [26] Y.-H. Wen, L. Gao, H. Fu, F.-L. Zhang, and S. Xia, "Graph cnns with motif and variable temporal block for skeleton-based action recognition," in *AAAI Conference on Artificial Intelligence (AAAI)*, vol. 33, no. 01, 2019, pp. 8989–8996. 3, 21
- [27] Y.-F. Song, Z. Zhang, and L. Wang, "Richly activated graph convolutional network for action recognition with incomplete skeletons," in *International Conference on Image Processing (ICIP)*. IEEE, 2019, pp. 1–5. 3, 21
- [28] C. Si, W. Chen, W. Wang, L. Wang, and T. Tan, "An attention enhanced graph convolutional lstm network for skeleton-based action recognition," in *Proceedings of the IEEE/CVF Conference on Computer Vision and Pattern Recognition*, 2019, pp. 1227–1236. 3, 5, 8, 18
- [29] Z. Huang, X. Shen, X. Tian, H. Li, J. Huang, and X.-S. Hua, "Spatio-temporal inception graph convolutional networks for skeleton-based action recognition," in *International Conference on Multimedia (MM)*, 2020, pp. 2122–2130. 3
- [30] K. Cheng, Y. Zhang, X. He, W. Chen, J. Cheng, and H. Lu, "Skeleton-based action recognition with shift graph convolutional network," in *Proceedings of the IEEE/CVF Conference on Computer Vision and Pattern Recognition*, 2020, pp. 183–192. 3, 5, 7, 18, 21
- [31] K. Cheng, Y. Zhang, C. Cao, L. Shi, J. Cheng, and H. Lu, "Decoupling gcn with dropgraph module for skeleton-based action recognition," in *Computer Vision—ECCV 2020: 16th European Conference, Glasgow, UK, August 23–28, 2020, Proceedings, Part XXIV* 16. Springer, 2020, pp. 536–553. 3, 5, 16, 18, 21
- [32] Y. Chen, Z. Zhang, C. Yuan, B. Li, Y. Deng, and W. Hu, "Channel-wise topology refinement graph convolution for skeleton-based action recognition," in *Proceedings of the IEEE/CVF International Conference on Computer Vision*, 2021, pp. 13 359–13 368. 3, 5, 8, 9, 21
- [33] M. Li, S. Chen, X. Chen, Y. Zhang, Y. Wang, and Q. Tian, "Actional-structural graph convolutional networks for skeleton-based action recognition," in *Conference on Computer Vision and Pattern Recognition (CVPR)*, 2019, pp. 3595–3603. 3, 9, 10, 18
- [34] L. Shi, Y. Zhang, J. Cheng, and H. Lu, "Two-stream adaptive graph convolutional networks for skeleton-based action recognition," in *Proceedings of the IEEE/CVF conference on computer vision and pattern recognition*, 2019, pp. 12 026–12 035. 3, 9, 10, 18, 21
- [35] X. Zhang, C. Xu, and D. Tao, "Context aware graph convolution for skeleton-based action recognition," in *Proceedings of the IEEE/CVF Conference on Computer Vision and Pattern Recognition*, 2020, pp. 14 333–14 342. 3, 8, 18
- [36] M. Wang, B. Ni, and X. Yang, "Learning multi-view interactional skeleton graph for action recognition," *IEEE Transactions on Pattern Analysis and Machine Intelligence*, 2020. 3, 11
- [37] F. Ye, S. Pu, Q. Zhong, C. Li, D. Xie, and H. Tang, "Dynamic gcn: Context-enriched topology learning for skeleton-based action recognition," in *International Conference on Multimedia (MM)*, 2020, pp. 55–63. 3
- [38] Y. Du, W. Wang, and L. Wang, "Hierarchical recurrent neural network for skeleton based action recognition," in *Proceedings of the IEEE conference on computer vision and pattern recognition*, 2015, pp. 1110–1118. 3, 12, 17
- [39] H. Wang and L. Wang, "Modeling temporal dynamics and spatial configurations of actions using two-stream recurrent neural networks," in *Conference on Computer Vision and Pattern Recognition (CVPR)*, 2017, pp. 499–508. 3, 11, 12, 14, 17, 18
- [40] C. Si, Y. Jing, W. Wang, L. Wang, and T. Tan, "Skeleton-based action recognition with spatial reasoning and temporal stack learning," in *European Conference on Computer Vision (ECCV)*, 2018, pp. 103–118. 3, 11, 12, 13, 14, 18



- [41] W. Zhu, C. Lan, J. Xing, W. Zeng, Y. Li, L. Shen, and X. Xie, "Co-occurrence feature learning for skeleton based action recognition using regularized deep lstm networks," in *AAAI Conference on Artificial Intelligence*, vol. 30, no. 1, 2016. 3
- [42] S. Song, C. Lan, J. Xing, W. Zeng, and J. Liu, "An end-to-end spatio-temporal attention model for human action recognition from skeleton data," in *Proceedings of the AAAI conference on artificial intelligence*, vol. 31, no. 1, 2017. 3
- [43] C. Xie, C. Li, B. Zhang, C. Chen, J. Han, and J. Liu, "Memory attention networks for skeleton-based action recognition," in *International Joint Conference on Artificial Intelligence*, 2018. 3
- [44] C. Caetano, F. Br mond, and W. R. Schwartz, "Skeleton image representation for 3d action recognition based on tree structure and reference joints," in *SIBGRAPI Conference on Graphics, Patterns and Image (SIBGRAPI)*. IEEE, 2019, pp. 16–23. 3
- [45] C. Wu, X.-J. Wu, and J. Kittler, "Spatial residual layer and dense connection block enhanced spatial temporal graph convolutional network for skeleton-based action recognition," in *proceedings of the IEEE/CVF international conference on computer vision workshops*, 2019, pp. 0–0. 3
- [46] C. Plizzari, M. Cannici, and M. Matteucci, "Spatial temporal transformer network for skeleton-based action recognition," in *International Conference on Pattern Recognition*. Springer, 2021, pp. 694–701. 3
- [47] W. Peng, J. Shi, Z. Xia, and G. Zhao, "Mix dimension in poincar  geometry for 3d skeleton-based action recognition," in *ACM International Conference on Multimedia (MM)*, 2020, pp. 1432–1440. 3
- [48] W. Peng, X. Hong, H. Chen, and G. Zhao, "Learning graph convolutional network for skeleton-based human action recognition by neural searching," in *The AAAI Conference on Artificial Intelligence (AAAI)*, vol. 34, no. 03, 2020, pp. 2669–2676. 3, 21
- [49] I. Lee, D. Kim, S. Kang, and S. Lee, "Ensemble deep learning for skeleton-based action recognition using temporal sliding lstm networks," in *Proceedings of the IEEE international conference on computer vision*, 2017, pp. 1012–1020. 3, 13, 15, 18
- [50] Q. Ke, M. Bennamoun, S. An, F. Sohel, and F. Boussaid, "Learning clip representations for skeleton-based 3d action recognition," *IEEE Transactions on Image Processing*, vol. 27, no. 6, pp. 2842–2855, 2018. 3
- [51] J. Liu, G. Wang, P. Hu, L.-Y. Duan, and A. C. Kot, "Global context-aware attention lstm networks for 3d action recognition," in *Conference on Computer Vision and Pattern Recognition (CVPR)*, 2017, pp. 1647–1656. 3, 13, 16, 17, 18
- [52] Y. Tang, Y. Tian, J. Lu, P. Li, and J. Zhou, "Deep progressive reinforcement learning for skeleton-based action recognition," in *Conference on Computer Vision and Pattern Recognition (CVPR)*, 2018, pp. 5323–5332. 3, 13, 15, 17, 18
- [53] P. Zhang, C. Lan, W. Zeng, J. Xing, J. Xue, and N. Zheng, "Semantics-guided neural networks for efficient skeleton-based human action recognition," in *Proceedings of the IEEE/CVF Conference on Computer Vision and Pattern Recognition*, 2020, pp. 1112–1121. 3, 14, 18
- [54] M. Liu, H. Liu, and C. Chen, "Enhanced skeleton visualization for view invariant human action recognition," *Pattern Recognition*, vol. 68, pp. 346–362, 2017. 3
- [55] P. Zhang, C. Lan, J. Xing, W. Zeng, J. Xue, and N. Zheng, "View adaptive neural networks for high performance skeleton-based human action recognition," *IEEE transactions on pattern analysis and machine intelligence*, vol. 41, no. 8, pp. 1963–1978, 2019. 3
- [56] Z. Qin, Y. Liu, P. Ji, D. Kim, L. Wang, B. McKay, S. Anwar, and T. Gedeon, "Fusing higher-order features in graph neural networks for skeleton-based action recognition," *arXiv preprint arXiv:2105.01563*, 2021. 3
- [57] C. Caetano, J. Sena, F. Br mond, J. A. Dos Santos, and W. R. Schwartz, "Skelemotion: A new representation of skeleton joint sequences based on motion information for 3d action recognition," in *2019 16th IEEE International Conference on Advanced Video and Signal Based Surveillance (AVSS)*. IEEE, 2019, pp. 1–8. 3
- [58] Z. Cao, G. Hidalgo, T. Simon, S. E. Wei, and Y. Sheikh, "Openpose: Realtime multi-person 2d pose estimation using part affinity fields," *IEEE Transactions on Pattern Analysis and Machine Intelligence (T-PAMI)*, vol. 43, no. 1, pp. 172–186, 2021. 3
- [59] T. N. Kipf and M. Welling, "Semi-supervised classification with graph convolutional networks," *International Conference on Learning Representation*, 2016. 4
- [60] K. Simonyan and A. Zisserman, "Very deep convolutional networks for large-scale image recognition," *arXiv preprint arXiv:1409.1556*, 2014. 5
- [61] S. Yan, Y. Xiong, and D. Lin, "Spatial temporal graph convolutional networks for skeleton-based action recognition," in *Thirty-second AAAI conference on artificial intelligence*, 2018. 7, 21
- [62] E. Jang, S. Gu, and B. Poole, "Categorical reparameterization with gumbel-softmax," *International Conference on Learning Representation (ICLR)*, 2017. 9
- [63] G. Lefebvre, S. Berlemont, F. Mamalet, and C. Garcia, "Blstm-rnn based 3d gesture classification," in *International conference on artificial neural networks*. Springer, 2013, pp. 381–388. 12
- [64] K. Kawakami, "Supervised sequence labelling with recurrent neural networks," *Ph. D. thesis*, 2008. 13
- [65] R. Zhao, K. Wang, H. Su, and Q. Ji, "Bayesian graph convolution lstm for skeleton based action recognition," in *Proceedings of the IEEE/CVF International Conference on Computer Vision*, 2019, pp. 6882–6892. 16, 17, 18
- [66] J. Liu, G. Wang, P. Hu, L.-Y. Duan, and A. C. Kot, "Global context-aware attention lstm networks for 3d action recognition," in *Proceedings of the IEEE Conference on Computer Vision and Pattern Recognition*, 2017, pp. 1647–1656. 18
- [67] K. Cheng, Y. Zhang, X. He, J. Cheng, and H. Lu, "Extremely lightweight skeleton-based action recognition with shiftgcn++," *IEEE Transactions on Image Processing*, vol. 30, pp. 7333–7348, 2021. 18